HHS Public Access

Author manuscript

Ann Biomed Eng. Author manuscript; available in PMC 2018 May 30.

Published in final edited form as:

Ann Biomed Eng. 2018 May ; 46(5): 684–704. doi:10.1007/s10439-018-1990-1.

Nitinol Stents in the Femoropopliteal Artery: A Mechanical Perspective on Material, Design, and Performance

Kaspars Maleckis, **Eric Anttila**, **Paul Aylward**, **William Poulson**, **Anastasia Desyatova**, **Jason MacTaggart**, and **Alexey Kamenskiy**

Department of Surgery, 987690 Nebraska Medical Center, University of Nebraska Medical Center, Omaha, NE 68198-7690, USA

Abstract

Endovascular stenting has matured into a commonly used treatment for peripheral arterial disease (PAD) due to its minimally invasive nature and associated reductions in short-termmorbidity and mortality. The mechanical properties of the superelastic Nitinol alloy have played a major role in the explosion of peripheral artery stenting, with modern stents demonstrating reasonable resilience and durability. Yet in the superficial femoral and popliteal arteries, even the newest generation Nitinol stents continue to demonstrate clinical outcomes that leave significant room for improvement. Restenosis and progression of native arterial disease often lead to recurrence of symptoms and reinterventions that increase morbidity and health care expenditures. One of the main factors thought to be associated with stent failure in the femoropopliteal artery (FPA) is the unique and highly dynamic mechanical environment of the lower limb. Clinical and experimental data demonstrate that the FPA undergoes significant deformations with limb flexion. It is hypothesized that the inability of many existing stent designs to conform to these deformations likely plays a role in reconstruction failure, as repetitive movements of the leg and thigh combine with mechanical mismatch between the artery and the stent and result in mechanical damage to both the artery and the stent. In this review we will identify challenges and provide a mechanical perspective of FPA stenting, and then discuss current research directions with promise to provide a better understanding of Nitinol, specific features of stent design, and improved characterization of the biomechanical environment of the FPA to facilitate development of better stents for patients with PAD.

Keywords

Femoropopliteal artery; Nitinol; Stent; Design; Peripheral arterial disease

FEMOROPOPLITEAL ARTERY OBSTRUCTIVE DISEASE

Atherosclerotic Disease in the Femoropopliteal Artery

Chronic obstruction of the femoropopliteal artery (FPA) is a common cause of peripheral arterial disease (PAD). The FPA provides the majority of the arterial blood supply to the

Address correspondence to Jason MacTaggart and Alexey Kamenskiy, Department of Surgery, 987690 Nebraska Medical Center, University of Nebraska Medical Center, Omaha, NE 68198-7690, USA. jmactaggart@unmc.edu, Alexey.Kamenskiy@unmc.edu.

lower extremity[18–70] and begins below the inguinal ligament as the common femoral artery that then branches into the superficial femoral artery (SFA) and profunda femoris artery in the proximal thigh. The SFA transitions into the popliteal artery (PA) at the level of the adductor hiatus—a tendinous channel between the adductor magnus muscle and the femur. The PA crosses the knee joint and then bifurcates into the anterior tibial artery and the tibioperoneal trunk. During limb flexion, the FPA undergoes extensive mechanical deformation, with twisting, bending and compression concentrated in severity to the region around the adductor hiatus and the below knee PA segments. These deformations are thought to play major roles in FPA wall injury and flow disturbance, key factors in the development and progression of lower extremity occlusive disease. [4,29,30,73,99]

Up to 90% of PAD cases are attributed to atherosclerosis,[18] with or without calcification. Thromboembolic phenomena are also frequently encountered but are most commonly associated with acute lower limb ischemia, usually treated with thrombus removal and systemic anticoagulation. Other conditions can also lead to arterial obstruction in the lower limb, such as aneurysm or congenital entrapments. Atherosclerosis is a chronic inflammatory condition of the artery wall that progresses through multiple stages. It starts with lesion initiation through endothelial damage, which can be triggered by multiple factors including mechanical stress, hemodynamic disturbance, metabolic derangements associated with risk factors, and different immune or inflammatory processes, such as elevations in oxidative stress.[70] The next stage involves formation of non-clinically significant intimal thickening, that can progress into hemodynamically significant fibroproliferative atheroma and, ultimately, advanced occlusive lesions.[10] Advanced lesions invade deeper layers of the arterial wall and have complex structures with usually rigid outer layers composed of collagen, elastin, smooth muscle cells, macrophages, foam cells, and lymphocytes, and a core that may contain lipids, necrotic cells, or calcium deposits. Unlike coronary plaques, PAD lesions are usually more fibrous and may contain significant amounts of calcium that often spreads within the tunica media.[57,58] Calcification in the lower extremity, particularly in the setting of diabetes mellitus or chronic kidney disease,[50,51,57,108] doubles cardiovascular mortality and quadruples the risk of amputation,[50,69] but the etiology of FPA calcification remains unclear and is an area of active research.[27,28,50,54,101,103]

Like coronary and cerebrovascular disease, PAD lesions can develop over long periods of time without producing symptoms. As lesions develop, the artery frequently remodels by increasing diameter[45] and wall thickness to balance the hemodynamic shear and intramural stresses[52,53,56] until a critical threshold is reached and the diameter is not able to widen further. Once this maximum compensatory dilation occurs, additional plaque growth results in progressively more severe vessel lumen narrowing. It is at this point that clinical symptoms typically start to appear, with the most common patient complaint being pain or weakness of the lower limb muscles during walking, a condition called intermittent claudication. The severity and progression of PAD is heavily influenced by systemic risk factors, most notably cigarette smoking and diabetes mellitus.[18] Cigarette smoking leads to more rapid progression of PAD[10] through multifactorial effects on the cardiovascular system, including direct endothelial cell damage.[70] Those with diabetes often have more advanced disease at presentation, including a higher likelihood of having chronic limb threatening ischemia (CLTI) involving ischemic ulceration or gangrene.[10] Often diabetic

patients suffer severe circumferential vessel calcification[28,57] and stiffening of the entire infrainguinal vascular tree with associated occlusive disease localized to the smaller vessels below the knee.[5]

Early intervention is critical in patients with CLTI because of the high risk of amputation in the absence of revascularization.[3] Though a significant number of PAD patients with intermittent claudication can see improvement in symptoms with conservative medical therapies and exercise programs, many patients eventually experience gradual worsening of their condition. [18] With progression of symptoms, up to 7% of patients request some sort of intervention, including endovascular therapy or revascularization *via* surgical bypass.[18] Endovascular intervention is frequently the preferred treatment method due to its minimally invasive nature and shorter recovery times compared with bypass surgery.[48] During endovascular therapy, the lesion is typically accessed remotely through an access point in the common femoral artery or less commonly from the brachial or pedal arteries, and a balloon angioplasty procedure is performed to fracture the plaque and dilate the artery. Shorter lesions may be treated with angioplasty alone but in cases involving complex lesions and flow-limiting arterial dissections, a permanent metal mesh tube, called a stent, is deployed to help maintain arterial lumen patency. Alternatively, atherectomy procedures that shave plaque from the inner wall of the artery are also sometimes performed with the purported advantage of plaque debulking and reduced requirement for stenting.

The choice between endovascular therapies and surgical bypass operations often involves complex decision making incorporating arterial anatomy, patient risk factors, and personal preferences of the patients and treating physicians. A key factor in the outcome and durability of the reconstruction method is the indication for the procedure, with more severely ill patients with CLTI demonstrating inferior reconstruction patency and life-expectancy compared to patients with intermittent claudication indications. For healthier patients requiring reconstruction for intermittent claudication, life expectancies may be substantially longer than those with CLTI, requiring greater durability in whatever method is chosen for revascularization.

Clinical Challenges with Stents in the Femoropopliteal Artery

The number of endovascular procedures for PAD in the United States continues to increase due to increases in the population of patients with PAD and their preference for minimally invasive procedures with shorter recovery times. Compared to open surgery, patency rates of FPA stents continue to be worse than in most other arterial locations.[1,21,48,113,114] Early studies examining first generation Nitinol stents were inconclusive in showing that PAD stenting improved clinical outcomes compared to other procedures such as balloon angioplasty or open bypass surgery.[83] Recently, many clinical trials (most are industry-supported) have claimed improved durability and patency of endovascular FPA stent-based repairs[109] demonstrating patency rates between 43% and 90% at 12 months (Table 1). Even with these recent improvements in FPA stenting, existing data demonstrate that bypass surgery still provides better results in terms of restenosis and freedom from reintervention, and similar results in terms of freedom from amputation. [15,26,115] Furthermore, endovascular

treatments of the in-stent restenosis (ISR) continue to disappoint showing high rates of recurrence.[67]

What is Unique About the FPA Environment?

Stents designed for different arterial beds need to accommodate various degrees of deformations, and in the FPA these deformations are some of the most severe in the body (Fig. 1). Studies that aimed to quantify the complex mechanical environment of the flexing limb can be roughly divided into those reporting baseline deformations of the FPA, and deformations of the stented FPA due to limb flexion.

Baseline FPA Deformations

Smouse *et al.*[119] was one of the first to evaluate deformations of the FPA with limb flexion. Utilizing seven human cadavers and 2D angiography, they imaged lower limbs in straight and bent configurations mimicking walking, sitting, and stair-climbing activities. Arterial bending and foreshortening were measured, and authors reported that FPA deformations were more severe distally in the PA below the knee than in the more proximal SFA.

The first study to use 3D imaging and measure torsion of the FPA due to limb flexion was performed by Cheng *et al.*[17] They used arterial side branches as markers to track deformations of the FPA as it deformed from supine to fetal positions, producing 60° ± 34° torsion and 13% ± 11% FPA axial compression. However, torsion values were not normalized to the length of the artery. Normalized values were published several years later by the same group[16] and constituted 1.3 ± 0.8–2.1 ± 1.3°/cm twist with higher values occurring distally.

In 2013, Ansari *et al.*[4] performed a literature review of the biomechanical environment of the FPA and found a total of 12 studies that evaluated FPA deformations with limb flexion. Though many of these studies reported disparate deformation measures, Ansari *et al.* concluded that the FPA experiences 2–4°/cm twist, 4–13% axial compression, and has 22–72 mm bending radius during limb flexion. Until recently these values summarized our current understanding of the FPA mechanical environment.

A new step in understanding of the true severity of arterial mechanical deformations in the flexing limb came recently with the introduction of the intra-arterial marker method.[73] Custom-designed Nitinol markers (Fig. 1c) were endovascularly deployed in the limbs of human cadavers without disturbing the surrounding tissues, and used to measure axial compression, bending, and twist of the artery with limb flexion.[73,99] Markers did not have any sizable effect on FPA deformations, yet allowed accurate and repeatable measurements. The advantage of using markers as opposed to arterial side branches was that branches are frequently small and difficult to identify using clinical CT or MR, which leaves large segments of the FPA with unknown deformations. In addition, side branches tether the artery to the surrounding tissues, resulting in smaller deformations at these anchoring points. Finally, use of cadavers allowed to measure longitudinal pre-stretch that is impossible to quantify without excising the artery.[58] These advantages of the marker method allowed to assess axial compression both with respect to *in situ* pre-stretched configuration, and with respect to stress-free *excised* configuration which showed appreciable differences.[29]

FPA deformations measured using intra-arterial markers were 2–7-fold larger than reported previously by Ansari *et al.*[4] Poulson *et al.*[99] reported 9–25% axial compression and 8–27 mm bending radii of the FPA as a result of limb flexion, and Desyatova *et al.*[30] reported 8–26°/cm twist depending on posture. In addition, FPA deformations were described as highly non-uniformly distributed along the length of the artery reaching high values at the adductor hiatus and below the knee PA—the two typical locations of FPA disease.[129]

Stented FPA Deformations

Though stent design profoundly influences stent-artery interaction, the effects of stent design on limb flexion-induced FPA deformations are insufficiently understood. The first two studies investigating stented FPA deformations were performed by Smouse *et al.*[119] and Nikanorov *et al.*[91] who used human cadavers, 2D angiography, and Nitinol stents deployed in different segments of the FPA. They reported FPA axial compression of 3–11% and bending angles of 4°–54° depending on position along the length of the artery with higher values observed distally. The same technique of 2D angiography was applied by Nikanorov *et al.*[90] to evaluate stented FPA deformations *in vivo*, and more recently by Gökgöl *et al.*[46] who acquired two2Dscans of each stented limb. Reported axial compression of the stented FPA segments was in the range of 3.1–8.5%, and distal to the stent reached 9.3%.[46] Bending radii within the stented segment ranged 135–22 mm depending on location, with many stents kinking in the flexed limb.[46] Ganguly *et al.*[43] measured deformations of the stented FPA in patients using 3D CTA and obtained similar results. Finally, Ghriallais *et al.*[89] reported that axial compression and curvature of the FPA change in the presence of the stent, with the amount of change dependent on stent characteristics. No studies were found to investigate torsion of the stented FPA.

Our team has recently performed assessments of axial and radial compression, bending, and torsion of the stented FPA using a perfused human cadaver model, seven commercially available FPA stent designs (AbsolutePro, Supera, Innova, Zilver, SmartControl, SmartFlex), and an intra-arterial marker method. Our data demonstrated significant differences in the ability of different device designs to accommodate limb flexion- induced deformations, but no device was able to accommodate all deformation modes without either restricting or exacerbating baseline deformations either within or outside the stented segment.[74]

FPA Stent Fracture

Severe mechanical environment of the FPA and cyclic deformations occurring with each limb flexion may result in stent strut fractures due to fatigue. While most patients with FPA restenosis do not have fractures in their stents,[64,131] PAD stent fractures are commonly thought to be associated with poor patency of PAD repairs as they occur more frequently in the FPA than in other arterial locations. Scheinert *et al.*[111] evaluated 121 limbs of patients who underwent SFA stenting and found fractures in 37% cases (45 legs). Authors reported that occurrence of stent fractures was related to the length of the stent and the number of implanted stents, with more fractures observed in longer and overlapping devices. Similarly Laird *et al.*[66] reported a 4.1% stent fracture rates in as early as 18 months after implantation. The extent of the stent damage by some investigators has been classified into five categories ranging from the fracture of a single strut, to fracture of multiple struts that results in a gap

between two parts of the stent.[85] Higher category fractures are reported to have higher rates of restenosis and complete occlusion than stents with mild fractures. Besides restenosis, FPA stent fractures can also lead to thrombosis, perforation, and migration of the stent increasing patient morbidity and potentially death. Adlakha *et al.*[2] and Schlager *et al.*[115] reported decreases in the rate of stent fracture with newer, second generation stents; however even with these newer devices, fractures were still observed.

Stent fractures are not usually considered the main culprit causing in-stent FPA restenosis, but they are likely reflective of the severe, repetitive deformations experienced in the FPA at, and around the stent, which likely play a role in reconstruction failure. The severe mechanical environment of the flexing limb that is able to fracture a metal stent, will also contribute to arterial injury resulting from the interaction of the FPA wall with the device, particularly if this device was not designed to accommodate the severity of limb flexion-induced deformations.[78,127]

While many biological factors also likely contribute to poor clinical outcomes of FPA stenting, mechanical stent characteristics and the severe biomechanical environment of the flexing limb seem to play important roles influencing device-artery interactions. A detailed understanding of stent characteristics is crucial for developing devices that perform well and can adapt to the unique biomechanical environment of the lower extremity arteries. We will review these characteristics starting with description of the unique features of the Nitinol alloy.

NITINOL ALLOYS

Currently, all FPA stents are metallic and remain permanently in the artery, although development of new bioresorbable polymer stents for the lower extremity is an area of active research.[102,116,132] All metallic stents are divided into two main categories— balloon-expandable stents that are usually made from stainless steel or cobalt–chromium, and self-expandable stents that are made from superelastic shape-memory alloys, typically Nitinol. Due to the severe deformations that the FPA experiences during limb flexion, balloon-expandable stents are usually not used in PAD repair as they may undergo irreversible plastic deformations (Fig. 2).[112] Most PAD stents therefore are made of self-expandable shape memory Nitinol that allows the device to expand to a pre-set shape once released from the catheter without the assistance of a balloon, and, most importantly, return to this shape after being deformed during limb flexion. While some Nitinol stents are also coated with drugs, i.e., paclitaxel, current review will focus on the mechanical rather than biological aspects of stent design and behavior.

A Brief History of Nitinol and Nitinol Stents

Nitinol was discovered in 1959 by William J. Buehler while working in the U.S. Naval Ordnance Laboratory in White Oak, Maryland.[60] The word Nitinol was derived from the combination of words nickel (Ni), titanium (ti), and Naval Ordnance Laboratory (nol).[14] The unique properties of Nitinol were discovered by accident while Buehler was experimenting with several binary alloys in his laboratory. While dropping hot and cold bars on a concrete floor to roughly determine the damping characteristics, he noticed a difference in sounds

between hot and cold Nitinol bars. Sparking his curiosity, these unexpected findings led to future research in which Buehler discovered that Nitinol had excellent fatigue resistance and other unique properties. While presenting a long strip of the alloy to colleagues, an accidental discovery of the shape-memory effect of the alloy occurred as the folded Nitinol strip was heated and stretched out to its original form. After years of further research, Nitinol's first successful use was in a pipe coupler for hydraulic fluid lines in an F-14 jet in 1969.[60] Since the alloy was never patented, its use in devices began to expand in other areas such as eyeglass frames, fire sprinkler systems, and other military and civilian applications. The first medical use of Nitinol occurred in orthodontic bridge wires in the late 1970's, and in 1989 the U.S. Food and Drug Administration (FDA) approved the use of a Nitinol anchor in orthopedic shoulder surgery. The first cardiovascular use of Nitinol was in a blood filter to trap clots,[60] and the first self-expanding Nitinol stent was developed and used in the aorta[23] and the FPAs[31] of dogs in 1983. Interestingly, the word stent was derived from Charles Stent, an English dentist born in 1807, and referred to a structure that supported facial skin grafts.

Structure and Thermal Properties of Nitinol Alloys

The unique properties of Nitinol arise from its crystal structure that can undergo specific phase transitions under mechanical or thermal events. Nitinol has two main phases with distinct features and characteristics. One of them is austenite phase, also called parent phase, which has a simple cubic B2 structure (Pm3m space group) with body centered atoms. The other phase is martensite phase, also called daughter phase, with a monoclinic B19' structure ($P2_1/m$ space group) that resembles herringbone pattern.[9,106] Both structures are shown in the left panel of Fig. 3. One of the ways to induce the transition between these two phases is through thermal flux. The martensite phase is present at lower temperatures, but it transitions to the austenite parent phase when Nitinol is heated above a certain temperature that varies based on Nitinol composition and manufacturing conditions. Specifically, the austenite-start (A_s) and austenite-finish (A_f) temperatures are the temperatures at which Nitinol begins and completes the transition to austenite phase upon heating, respectively. Transition from martensite to austenite is accompanied by small (< 1%) volume decrease, resulting in negative dilation. The martensite-start (M_s) and martensite-finish (M_f) temperatures correspond to the temperatures at which Nitinol begins and completes transition to martensite phase upon cooling, respectively. The transition from martensite to austenite occurs at higher temperature than transition from austenite to martensite. As a result, thermal transition curves exhibit the characteristic hysteresis during thermal transition cycles (Fig. 3, left panel). In cold worked and aged Nitinol alloys, thermal transitions between austenite and martensite phases may also occur through a third, rhombohedral phase or R-phase. The unit cell of R-phase has $P\bar{3}$ symmetry[94,118] and it appears as a distortion of the cubic austenite cell that has been elongated diagonally in the [111] direction [34] as illustrated in Fig. 4.

There are several factors that affect the phase transition temperatures of Nitinol, including heat setting temperature, time, and cooling rate during manufacturing. Also of importance is the chemical composition of Nitinol, i.e., the exact ratio of nickel to titanium (Fig. 3, right panel), as well as how the alloy is created, processed, and cold-worked to its final, raw form.

[38,62] Yeung *et al.*[134] determined that austenite transition temperatures decrease when ageing temperature is increased in the 400–550 °C range, while ageing time and cooling rate showed minor effect on austenite transition. Since austenite transition temperature can be tuned to the human body temperature, stent delivery procedures can benefit from the phase transition-driven superelastic and shape memory properties, and Nitinol stents can expand to a set shape once released from the catheter without the assistance of a balloon.

Mechanical Properties

Mechanical properties of Nitinol are governed by its temperature-dependent microstructure. The superelastic mechanical properties of Nitinol are present only between the A_f and M_d (martensite forming) temperatures when Nitinol is in its austenite form. Unlike typical metal alloys that have recoverable deformability below 1%, elastic recovery of Nitinol in the superelastic temperature range ($A_f < T < M_d$) can reach up to 10% strain.[96,106] This deformation, however, is significantly different from the traditional linear- elastic response of metals and alloys. The stress-induced phase transitions between austenite and martensite phases play key roles in Nitinol's superelasticity. As shown in Fig. 5, superelastic Nitinol deforms in a highly non-linear fashion with four distinct stages and significant hysteresis. The first stage of deformation is linearly elastic with relatively high modulus, and it is caused by the deformation of chemical bonds in austenite microstructure. At about 1% strain, the second yield-like deformation stage starts and continues up to 7% strain with a minor increase in stress. However, unlike plastic yielding, during which unit cells irreversibly slip with respect to each other, this deformation results from the phase transition from austenite to a twinned martensite structure (in twinned crystal structures part of the parent phase is reoriented into its mirror configuration due to the shear stresses). The third stage of deformation is elastic detwinning of the martensite phase during which the mirror-like twinned structure is stretched out to a single orientation. This deformation stage is characterized by the increase in modulus. The elastic deformation is followed by stage four, which is a plastic deformation of the martensite phase until failure. Deformations in the first three stages are fully recoverable, although the forces during unloading are smaller than during loading as a result of hysteresis. The unique biomechanical characteristics of stents associated with the hysteresis are discussed in ''Mechanical Properties''.

Both the austenite finish (A_f) and the martensite forming (M_d) temperatures that bound the superelasticity range, depend on material composition and heat treatment during manufacturing. If the temperature is higher than M_d, the critical stress or energy of austenite to martensite transformation is higher than that of the dislocations, and Nitinol follows a traditional alloy-like plastic deformation after stage I. Although Nitinol can be completely austenitic between the M_s and A_f temperatures (depending on its thermal history), it is not able to recover large deformations during mechanical loading cycle. However, this plastic-like deformation can be fully recovered once Nitinol is subjected to a thermal cycle above the A_f temperature, which is called the shape-memory property. Furthermore, below the A_f temperature, the stress-induced austenite to martensite transition can occur through the R-phase (A → R → M), that appears as a narrow plateau in the deformation stage I (Fig. 4). The critical stress for the A → R transition increases with the increase in temperature and eventually exceeds the critical stress for the A → M transition as temperature reaches the

A_f. On the stress–strain curve, this shows as an upwards migration of the R-phase plateau until A → R and R → M merge into a single A → M transition.[88]

Different manufacturing techniques influence the microstructure of Nitinol and can be used to tailor the mechanical properties to specific applications. Hot or cold working is one of such techniques that can increase dislocation density, resulting in hindering of material reorientation and increase of critical stress for martensite transformation. Both hot and cold workings also induce formation of crystallographic textures along ⟨110⟩ and/or ⟨111⟩ unit cell directions, which further increase transformation stresses.[41]

Another important manufacturing parameter that influences Nitinol mechanical properties is the temperature of thermal treatment. An increase of this temperature induces the growth of Ni_4Ti_3 precipitates, which can impact the mechanical properties of Nitinol in different ways. For example, formation of large precipitates was shown to reduce stress for martensite transformation, while small coherent precipitates induce Nitinol hardening as they effectively prevent dislocation motion.[41] Similarly, the precipitates and their development also affect thermal properties of Nitinol due to depletion of the Ni atoms from the alloy matrix. In particular, longer heat treatment times result in formation of precipitates with higher Ni content (Ni_3Ti_2 and Ni_3Ti) that result in substantial increase of A_f transition temperature.[32,92] The effects of precipitate growth however are reversed when ageing temperature reaches 600 °C due to dissolution of the precipitates.

Biocompatibility

Biocompatibility refers to the ability of the material to perform in a specific application with an appropriate host reaction. The main concerns of metal alloy biocompatibility are typically related to the corrosion resistance and toxicity of the individual chemical elements. Pure titanium is biocompatible due to its ability to form stable oxide layer. On the contrary, pure nickel in high concentrations is known to cause systemic toxicity, cellular damage, and immune response in patients with nickel sensitivity.[38] Previous *in vitro* and *in vivo* studies reported that formation of the stable titanium oxides (TiO_2) and nickel oxides (NiO and Ni_2O_3) prevent nickel ion exposure and diffusion into cells[110] and that surface-finished Nitinol releases only a small amount of nickel into the blood, generally less than 10% of the average dietary intake.[35] However, a recent study showed that oxide layers created by some surface treatment methods might not be as stable as previously thought.[123] In particular, a strong positive correlation between oxide layer thickness (from various methods of surface treatment) and nickel ion release was found. Furthermore, it was shown that severe mechanical deformations that Nitinol devices normally experience during deployment and function can further increase the release of nickel from the Nitinol alloy as oxide layers lack the superelastic mechanical properties and develop cracks under large strains.

NITINOL STENTS

Manufacturing Approaches

Due to Nitinol's superelastic properties, manufacturing complex Nitinol devices using conventional cutting or machining tools can be difficult and cause substantial tool wear.[38] In

addition, Nitinol stents usually have intricate patterns, which are difficult to cut to their final configurations. To overcome the challenge of tooling, Nitinol stents are manufactured either by laser-machining from a tube or by knitting or braiding individual wires. Although wire-based stents historically were the first type of Nitinol stents used, their disadvantages are increased wall thickness and accelerated wear due to crossing of the filaments. [121] Laser-machined stents can be either pre-cut or pre-expanded. Pre-cut stents are made from a tube that has smaller diameter than the end-product. The shape and properties of the final pre-cut stent are formed by mechanical expansion and heat treatment procedures that are repeated several times. This results in heterogeneous microstructure and properties compared to pre-expanded stents as expansion causes inhomogeneous stress state in the stent elements.[39]

Pre-expanded stents are laser-cut from a tube that has the final stent diameter, and the device undergoes a single heat-treatment. The heat treatment is one of the most important steps of Nitinol stent manufacturing as it sets the final shape and properties of the stent. Nitinol is shape-set by deforming the sample into a desired geometrical shape, and heating it to high temperatures (on the order of 450–550 °C). Nitinol stents are shape-set in the open form so they can return to it (i.e., self-expand) when released from the catheter during deployment.[72] For self-expansion to occur, the A_f of the stent must be lower than the human body temperature so when the device is deployed in the artery it is in the austenitic, superelastic form. Understanding the precise heating and cooling methods is therefore necessary to control structure and properties of the final product. Liu *et al.*[72] showed that the optimal shape-setting temperature is 450–500 °C for 50.7% nickel Nitinol wire and that heating time should be longer than 10 min, but no longer than 60 min to retain maximum deformation recoverability and to achieve high superelasticity.

In addition to laser-cutting and shape-setting, Nitinol stents usually require further processing to remove excess alloy, smooth edges, remove heat affected zones caused by laser cutting, and enhance biocompatibility by creating stable oxide layer.[38] In addition, electropolishing is commonly used to provide a high luster to the stent and improve its fatigue life through removal of microdefects.

Geometry

Nitinol stents vary significantly in length, diameter, strut thickness, and design. Stents used in the FPA typically have diameters between 5 and 8 mm and are usually slightly oversized compared to the diameter of the artery. In certain instances such as with a braided stent, no oversizing may be recommended because resistance to radial compression is significantly reduced when the braided stent is extended beyond its nominal length. Stent lengths can vary significantly, usually in a range 20–250 mm depending on the length of the lesion to be covered. With different manufacturers, there are currently a wide variety of strut thicknesses, patters (Fig. 6) and shape-set conditions, which lead to a wide variety of physical and mechanical characteristics.[78] Nevertheless, all Nitinol stents possess similar non-linear and superelastic shape-memory behavior intrinsic to the Nitinol alloy.

Mechanical Properties

The mechanical properties of the Nitinol alloy provide unique biomechanical characteristics to stents. Due to the shape memory effect, Nitinol stents ‘‘self-expand’’, i.e., they are deployed without the use of an expanding balloon. In addition, mechanical hysteresis behavior of Nitinol results in a unique mechanical feature called ‘‘biased stiffness’’, which means that a stent that recovers from the crimped position will be much more resistant to compression than to expansion, as illustrated in Fig. 7. Since conventional z-shaped Nitinol stents are frequently oversized to account for the overstretched lumen after angioplasty, ‘‘biased stiffness’’ is useful for reducing the outward force. However, due to its constant action, outward force that results from significantly oversized Nitinol stents still possess a potential risk of damaging the vessel wall.[36] To minimize this damage, several key characteristics described below need to be taken into account when designing Nitinol stents.

Radial resistive force (RRF) and Chronic outward force (COF) are the two main characteristics that determine the force balance between the vessel wall and the stent. RRF is a measure of the amount of force required to compress the stent radially, while COF correlates to a measure of the radial force the stent projects outward in its deployed configuration. Both RRF and COF are determined by the unique force hysteresis of Nitinol and they are the two most commonly researched stent characteristics.

Hoop strength is another important design parameter that defines the maximum hoop load that can be carried by the stent. Hoop stresses in a cylindrical stent can be estimated by using the thin-walled pressure vessel equation:

$$\sigma = \frac{\rho \cdot d}{2 \cdot t}, \quad (1)$$

where ρ is pressure, d is diameter, and t is wall thickness. Failure of the stent can occur when hoop stress exceeds the material strength. Hoop strength is directly proportional to the cross-sectional area of the device, which is linearly proportional to the width and thick-ness of the stent struts. Sometimes hoop force, F_{d}, or hoop force per unit length, f_{d}, is used instead of hoop stress to characterize load acting on the stent:

$$F_{\mathrm{d}} = \sigma \cdot L \cdot t = \frac{\rho \cdot d \cdot L}{2}, \quad (2)$$

$$f_{\mathrm{d}} = \frac{F_{\mathrm{d}}}{L} = \frac{\rho \cdot d}{2}, \quad (3)$$

where L is stent length.

Hoop stiffness is defined as the hoop force per diameter change:

$$K_{\mathrm{d}} = \frac{F_{\mathrm{d}}}{\Delta d}, \quad (4)$$

Hoop stiffness depends on stent geometry and has a linear relation to strut thickness, cubic relation to strut width, and an inverse cubic relation to the strut length[36]:

$$K_{\mathrm{d}} \propto \frac{Ew^3 t}{n(L_{\mathrm{s}})^3}. \quad (5)$$

In addition to hoop stiffness, pinching stiffness is also used in stent design. It is defined as a resistance of the stent to deformation or buckling when it is compressed between two parallel plates. Under pinching load, stent struts are subjected to out-of-plane bending. Unlike the hoop stiffness, pinching stiffness has linear dependence on strut width, but cubic dependence on strut thickness.[36] Other important characteristics for stent design include bending stiffness, and stiffness in axial tension and compression that are also functions of strut geometry, number of interconnectors, and angles between them.

DESIGN CONSIDERATIONS FOR IMPROVED MECHANICAL PERFORMANCE

Mechanical stent performance is a function of the intrinsic characteristics of the stent and the biomechanical environment in which the device functions. When the two are clearly defined, computational modeling can be used to simulate complex *in vivo* loading conditions and optimize device performance.

Benchtop Mechanical Characteristics of Stents

A major step towards improved stent design is better understanding of the stent mechanical characteristics. Although general properties of raw Nitinol are well studied, the exact mechanical characteristics of processed Nitinol used in devices of different manufacturers are proprietary.

There are two fundamentally different types of mechanical testing of Nitinol stents. The first is utilized by stent manufacturers to satisfy the requirements of the FDA in order to get device approval. The results of this testing are usually proprietary, but the FDA provides a comprehensive non-binding guidance for the manufacturers,[40] including specific testing methods and standards to use for mechanical and fatigue testing, and computational modeling of stents. Many ASTM standards are referenced for common testing methods such as ASTM F2477 which lists guidance on pulsatile durability testing.[6] ASTM standards are very specific with given testing parameters and specific equipment, but are not all-inclusive. For example, axial compression, torsion, and bending tests of Nitinol stents are currently not standardized by the ASTM.

The second type of mechanical testing is performed to compare the performance of several devices under different mechanical loading conditions or to reverse-engineer stent properties. Results of these tests can be found in the literature published by both industry and academic research groups. Several testing modes are usually utilized, and those include radial compression, crush resistance, bending, axial tension and compression, and torsion, all done either quasi-statically or under cyclic dynamic loading (Fig. 8).

Radial Compression

Radial compression tests are performed to evaluate RRF and COF of Nitinol stents. Stents can either be tested as separate structures, or, more frequently, deployed inside compliant (usually silicone) tubes to simulate oversizing. Testing is typically performed at 37 °C and equipment to measure resistance to radial compression consists of a load cell, a thin myler-sheet loop used to wrap around the stent, a roller, and a base post.[33,47,121] The most typical design is demonstrated in Fig. 8 although alternative setups have also been described.[47] Duda *et al.*[33] measured RRF of 8 mm-diameter Nitinol stents with high strength polyester film that was looped around the stent. The results were expressed as force per unit length that is required to reduce the diameter of the stent to 6 mm. The average radial resistive force was 137 N/m for the Symphony stent, 127 N/m for the Memotherm stent, and 165 N/m for the Smart stent.

Recently, Maleckis *et al.*[78] compared radial resistance of 12 currently used FPA Nitinol stents (Absolute Pro, Supera, Lifestent, Innova, Zilver, Smart Control, Smart Flex, EverFlex, Viabahn, Tigris, Misago, and Complete SE).[78] Stents were compressed with a modified v-shaped clamp setup that applied compression from four sides simultaneously. Supera stent had the highest radial stiffness of 11,261 N/m when compressed to 90% of its initial cross-sectional area. Apart from the Supera stent, the Complete SE, LifeStent, and Viabahn stents demonstrated high radial stiffness (> 700 N/m), while Smart Control and Zilver stents were relatively weak radially (< 300 N/m). LifeStent, Innova, SmartControl, EverFlex, Misago, and Complete SE stents lost most of their radial stiffness when they were compressed beyond 65–70% of their initial cross-sectional area. A moderate drop in radial stiffness under significant radial compression was also observed for the Absolute Pro and Viabahn stents, while stiffness of the Zilver, Smart Flex, and Tigris stents increased with higher levels of radial compression.

Although these bench-top tests give valuable insights into the ability of different stents to resist pinching, more realistic radial compression tests involving Iris-type mechanisms that engage the entire circumference, and deployment in artery-like tubes with oversizing is needed to replicate the *in vivo* conditions.

Crush Resistance

Another test that is similar to radial compression, is testing for stent crush resistance.[47] In crush resistance testing, the stent is squeezed between the two parallel surfaces instead of being uniformly compressed around the circumference. This type of test is sometimes preferred over radial compression due to its simplicity, but loading conditions are obviously different than those in radial compression. Consequently, the results of these two tests

cannot be compared directly. In a report of stent mechanical properties by GORE,[128] it was shown that there are significant differences in crush resistance between different stent models. In particular, the highest resistive force associated with 25% lateral compression of a two-inch-long section of a 6 mm-diameter stent was reported for Fluency Plus (296 g), followed by Protégé GPS (242 g), Cordis Smart (153 g), Bard Lifestent NT35 (150 g), Gore Viabahn (125 g), and Absolute stents (115 g). Dyet *et al.*[37] measured crush resistance of 8 mm-diameter stents using a variation of technique presented in Fig. 8 by compressing the stents between a support plate and a 6.35 mm-diameter micrometer head. Compression strength of Instent Vascucoil (Medtronic), Symphony (Boston Scientific), and Memotherm (Bard) stents (all 40 mm long) was measured as force in Newtons that is required to compress the stent to 50% of its nominal diameter. Instent Vascucoil, and Memotherm stents showed 2.7 N resistance, while Symphony showed 3.4 N resistance.

Bending

Bending characteristics of FPA stents are typically obtained with a three-point bending setup (Fig. 8). GORE compared resistive force of 6 mm-diameter stents with 45 mm spans deformed to 5 mm in the middle of the span. Their results showed that Viabahn had the least resistance to bending (0.5 g), followed by Absolute (1.9 g), and Lifestent NT35 (2.2 g) devices. Significantly higher resistances were observed for the Smart stent (17 g), Protégé (38 g), and Fluency Plus (54 g) stents. Results also showed that Fluency Plus, Protégé GPS, and Smart stents collapsed laterally under severe bending conditions, while Viabahn, Absolute, and Lifestent NT35 maintained an open cross-section.

Dyet *et al.*[37] used a manual reduction gearbox-based device to determine bending properties of 8 mm-diameter Instent Vascucoil, Symphony, and Memotherm stents (all 40 mm long) subjected to bending deformations. Bending stiffness was measured as force in Newtons that is required to induce 10° bending of a 20 mm long section of a stent. Instent Vascucoil showed 5 mN bending stiffness, Memotherm stent showed 200 mN bending stiffness, and Symphony showed 490 mN bending stiffness. They also noted that at higher flexions some of the stents kinked.

Duda *et al.*[33] compared 8 mm-diameter stents under bending deformations by comparing the force needed to push a stent through a 120° bend of a Plexiglas tube. They showed that some of the stent designs have significantly different bending characteristics, but it was not clear how well this test described bending properties of stents as other conditions (i.e., friction) may have influenced the results.

Bending analysis of 12 FPA stents was also performed by Maleckis *et al.*,[78] and the data demonstrated large differences in bending stiffness between devices. Smart Control (98 N/m), Smart Flex (54 N/m), and EverFlex (46 N/m) had the highest bending stiffness, while Tigris (2 N/m), Viabahn (3 N/m), and Misago (10 N/m) stents had the lowest. In addition, they have also observed pinched diameters (Innova, Zilver, Smart Control, EverFlex, and Complete SE stents) and ‘‘gator-back’’ appearance of some devices (i.e., Absolute Pro, Misago, and Zilver) with struts pointing away from the stent and towards the arterial wall when the device was bent. Pinching typically occurred in stents that had short axial strut connections, while ‘‘gator-back’’ was observed in devices that had overall longer struts.

Axial Tension and Compression

Data on axial tension and compression testing are scarce in the literature. Favier *et al.*[39] performed axial tensile tests of custom-made uncut Nitinol tubes with different ageing treatments. Although stress–strain curves showed the characteristic non-linear behavior and high recoverable strains, it is not clear whether these properties translate into the mechanical behavior of the actual stents.

GORE reported a large variation of axial compression resistance of different stents at 15% compressive strain. In order to prevent stent buckling during the compression, stents were supported by an internal rod (Fig. 8). The lowest resistance was recorded for Viabahn (17 g), followed by Lifestent (54 g), Absolute (55 g), Smart (203 g), Fluency Plus (477 g), and Protégé GPS (539 g) stents. They also showed that Viabahn was the only design that did not buckle at 25% axial compression.

Study by Maleckis *et al.*[78] demonstrated that tensile stiffness of 12 currently used FPA stents varies significantly, with Viabahn, Smart Flex, and Tigris being the stiffest (12,387, 2469, and 2398 N/m tensile stiffness, respectively), and Misago, Absolute Pro, and Supera being the most compliant (32, 47, and 94 N/m tensile stiffness, respectively) under tension. For Viabahn and Tigris devices high stiffness in tension was caused by ePTFE fabric and plastic interconnectors rather than the wire Nitinol elements. Similarly, FPA stents also showed large differences in axial compression with Smart Control, Smart Flex, and Zilver stents being the stiffest (534, 236, and 218 N/m compressive stiffness, respectively), and Tigris and Viabahn being the softest in compression (both 7 N/m), likely due to helical design of their Nitinol wire. Furthermore, Smart Flex, EverFlex, Innova, Smart Control, Complete SE, and Zilver stents buckled when axially foreshortened by 25%, which corresponds to the physiologic compression experienced by the popliteal artery during limb flexion. Buckling instabilities involve sudden and large out-of-plane deformations, which may damage the arterial wall, and contribute to lower patency and faster mechanical device failure.

Torsion

Typical torsion setup used in stent characterization is demonstrated in Fig. 8. GORE[128] compared torsion characteristics of stents under 3°/cm rotation. Their results showed that the lowest resistance to torsion was observed for Absolute (1.2 g), followed by Lifestent NT35 (2.5 g), Viabahn (4.3 g), Smart (6.2 g), Protégé (9.6 g), and Fluency Plus (27.1 g) devices. Although this report gives a good comparison of differences in torsional performance for different stents, the testing conditions were significantly lower than physiological twist experienced by the FPA (26°/cm as opposed to 3°/cm).

Physiological levels of FPA twist were applied in a study by Maleckis *et al.*[78] where significant differences between 12 FPA stents were observed. The stiffest stent in torsion was Supera (959 μN m/°), likely due to its braided design and friction between the Nitinol wires. Smart Control (87 μN m/°) and Smart Flex (58 μN m/°) were also among the stiffest, while the least stiff stents were Viabahn (2 μN m/°), Absolute Pro (9 μN m/°), and Tigris (13 μN m/°) devices. Furthermore, Supera, Lifestent, Smart Flex, and EverFlex stents buckled before reaching upper levels of physiologic twist. High resistance to torsion, and buckling

during twist are both promoting adverse interactions between the arterial wall and the device, potentially leading to arterial wall injury and contributing to treatment failure. Smart Flex, Misago, and LifeStent also showed significant differences between clockwise and counter-clockwise rotations due to their non-symmetric designs.

Cyclic and Fatigue Testing

Fracture of Nitinol stents has been attributed to the progression of cracks that are caused by cyclically-induced stress concentrations around microstructural defects. Despite its superelastic nature, Nitinol exhibits a low fatigue threshold compared to most other metallic and intermetallic materials. In 10 years FPA stent is expected to undergo about 420 million loading cycles due to heartbeat-induced pulsations, and about 18 million cycles from musculoskeletal motion during walking. The large number of loading cycles leads to accumulated fatigue damage and crack propagation, eventually resulting in strut fracture. Several investigators have characterized fracture mechanisms and fatigue properties of Nitinol. Robertson *et al.*[107] used synchrotron X-ray micro-diffraction and showed that in annealed flattened Nitinol tubes transformation from austenite to martensite phase takes place along the tip of the crack. This transformation leads to volumetric change, which is thought to further promote crack propagation due to induced additional tensile stresses.[120] It was also shown that crystallographic texture plays significant role in crack propagation with energetically preferred orientation at about 45° from the drawing direction in Nitinol tubes.[105] Furthermore, there is evidence that thickness of the Nitinol sample also plays an important role in fatigue resistance.[107] Consequently, process parameters and sample geometry are expected to have profound influence on fracture properties, therefore fatigue resistance may vary significantly between different stent designs.

Several studies investigated durability and fracture resistance of different stents under various types of loads. Muller-Hulsbeck *et al.*[82] performed fatigue testing of seven FPA stent designs in air at 37 °C and under 40% compression, 40° bending, and 30°/cm torsion. Stents were subjected to 5000–650,000 loading cycles, and the observed fracture rates are summarized in Table 2.

Another assessment of stent fatigue was performed by Nikanorov *et al.*[91] who used specialized axial compression and bending equipment designed by Abbott Vascular to test six stent designs. Stents were deployed into silicone tubes with oversize ratio of 1:1.4 and tested under 5% axial compression and 48° bending deformations in 37 °C saline solution for up to 10 million cycles at 7 Hz frequency. Stents were inspected for fractures every 24 h using an optical microscope. The results of these tests are summarized in Table 3.

A number of authors have also investigated fatigue testing of Nitinol stent components.[77,82,91,96] Pelton *et al.*[96] tested mechanical fatigue of custom-made diamond shaped V-strut sections. The diamond shaped specimens were fatigue tested at 50 Hz up to 10 million cycles or until fracture. The results showed linear correlation between the number of cycles the stent survived the loading and the amplitude of the applied strain when plotted on a semilogarithmic scale. However, the majority of samples survived all 10^7 cycles.

Mahtabi *et al.*[76] used martensitic phase Nitinol tubes for fatigue testing utilizing a combined axial-torsion method at room temperature and 0.1 Hz frequency up to 10^5 cycles. They showed that fatigue lives are significantly shorter for out-of-phase torsion-bending mode when compared to in-phase bending-torsion or pure torsion under equivalent von Mises stress criterion. They also reported complex crack propagation paths for in-phase axial-torsion specimens, suggesting dominant effects of axial stresses in crack propagation. These results suggested that more comprehensive experimental and analytical studies are needed to better understand Nitinol fatigue behavior under multiaxial loading conditions.

While these and other studies have significantly improved our understanding of fatigue properties of Nitinol, FPA stents continue to fail despite being engineered to provide a 10-year lifetime. Comprehensive studies that identify how material properties and specific design features influence mechanical performance, as well as fatigue testing with more realistic loading conditions, could potentially lead to novel FPA stent designs with improved fatigue performance.

Need for New Characterization Techniques

Bench-top mechanical tests of Nitinol stents give valuable insights to how different devices compare under controlled loading conditions. However, these tests cannot be directly used to identify specific design features that contribute to better mechanical performance as stents vary in multiple design parameters (and likely material properties) at the same time. Finite Element Modeling (FEM) can be used to determine these design features, but it requires knowledge of the material properties that are often proprietary. Mechanical properties of Nitinol can potentially be extracted through mechanical tests of individual struts; however such task is not trivial due to small dimensions and curved geometry. Alternatively, such data can be obtained through inverse computational methods, but large number of parameters that describe Nitinol properties prevents unique parameter determination. Additional research is therefore needed to determine exact material properties of Nitinol used in different FPA stents, unless these properties are provided directly by device manufacturers.

In addition to studying design features that promote better mechanical performance of FPA stents, device assessments should also include evaluating damage that stents inflict on the arterial wall, either through producing locally high stress concentrations, or abrasions that can cause endothelial injury or strut protrusion. Though to our knowledge, no correlation between specific stent features and clinical performance has yet been identified, bringing bench-top tests closer to *in vivo* conditions may help identify these design characteristics. However, since clinical performance is a function of many variables, many of which are patient-, rather than device-specific, stent assessments should likely include a combination of bench-top, animal model, and computational experiments[126] that need to be performed synergistically and evaluated by clinical trials.

Computational Assessment of Stent Behavior

FEM is widely used in design and development of FPA stents as it provides a cost-effective way to analyze stent performance under different loading conditions prior to bench-top

testing. In addition, FEM is the only way to assess stresses resulting from complex interactions between the arterial wall and the stent. Latter obviously requires accurate knowledge of the arterial mechanical properties, which for the FPA have recently been described in great detail.[28,55,56,58,59] A comprehensive constitutive model that describes the complexities of Shape Memory Alloy (SMA) behavior, and accurate mechanical properties of Nitinol are obviously also important to make simulations realistic.

One of the first attempts to describe SMA behavior was performed by Brinson and Lammering[13] who developed a non-linear FE procedure for a one-dimensional material. This procedure included a thermodynamically- derived constitutive model that utilized internal variables (material parameters) to account for pseudoelasticity and shape memory effect (SME) at all temperatures, loading conditions, and stress levels. The model was expanded by Boyd and Lagoudas[12] who exploited Gibbs free energy function and a dissipation potential to describe pseudoelasticity and the shape memory effect.

A different approach to modeling SMA based on its microstructural features was taken by Sun and Hwang.[124] They linked inelastic SMA deformations under mechanical or thermal loadings to a temperature, stress state, and loading history using a micromechanical approach. Patoor *et al.*[95] improved this model by introducing a new homogenization method that more accurately described the behavior of single crystals. A single crystal constitutive relationship was developed in order to provide a kinematic description of the martensitic phase transformation to better understand the physical mechanism behind it. Numerical simulations using this micromechanical model were in good agreement with experimental data and were able to provide details on the evolution of the microstructure during loading processes. Comstock *et al.*[20] further improved this micromechanical model by introducing arbitrarily imposed strains on the crystal instead of axisymmetric strains. This allowed to describe austenite to martensite transformation due to large stresses experienced by the SMA during its austenite phase and within any given temperature range.

More details on different constitutive models used to describe SMA behavior are provided in an article by Cisse *et al.*,[19] but it is evident that current SMA formulations do encompass the behavior of Nitinol quite well. However, they are based on many material parameters that are most often empirically derived. The type of testing to determine these parameters, temperature conditions, and even type of sample (i.e., wire, sheet, tube) all play a role and can significantly influence the variance in mechanical properties and computational results. Continued refinement and standardization of testing techniques, verification, and validation of computational models with bench-top experiments are therefore crucial.

One of the first attempts to validate computational SMA results with experiment was performed by Pelton *et al.*[97] They conducted an experimental analysis of the bending behavior of Nitinol wires and microtubes to verify FE simulations. Experimental assessments included uniaxial tension, compression, and three-point bending, which agreed well with FE even when the latter used a non-linear Ogden hyperelastic model built into ABAQUS (Simulia, Dassault Systemes, Waltham, MA). Multiple similar studies followed to describe one, two and three-dimensional behavior of Nitinol, culminating in a study done by Whitcher,[133] which provided one of the first descriptions of how to incorporate Nitinol

mechanical properties into FE to assess stent *in vivo* loading conditions. The goal of Whitcher's work was to predict the material fatigue life through FE calculations using Von Mises yield criterion and an elastic–plastic material formulation in ADINA (ADINA R&D, Watertown, MA). Since loading conditions were isothermal, no explicit SMA formulation was employed and the model lacked superelastic unloading. Cyclic pressure difference between systole and diastole was used to load the model. FE results were in good agreement with experimental fatigue testing, both within the testing range and until ultimate failure.

Since Whitcher's publication, many more studies investigated Nitinol stents under FE simulated physiologic loading conditions. Several of the recent studies that pertain to FPA stents were performed by Petrini *et al.*,[98] Conti *et al.*,[22] and Muller-Hullsbeck *et al.*,[82] Petrini *et al.*[98] studied peripheral Nitinol Bard Lifestent under limb flexion-induced deformations of the FPA. They were able to simulate strut fatigue due to bending, extension and compression loadings. Though the study was limited to a single case, authors concluded that FE can be used to study the mechanisms of stent fracture *in vivo*. Conti *et al.*[22] studied the effect of limb flexion-induced FPA deformations on a Nitinol stent incorporating patient-specific anatomy. This study concluded that the stress–strain field is non-uniform along the length of the stent, exposing certain areas of the stent to higher probability of fracture. Muller-Hulsbeck *et al.*[82] conducted FE analysis of seven FPA stents (Misago, Absolute, Smart, Luminexx, Sentinol, LifeStent, and Sinus-SuperFlex), and reported significant differences in strains associated with bending, compression, and twisting of the devices.

Currently, most well-known commercial FE software packages include SMA formulations as built-in material models which greatly facilitate studies like those described above. In ABAQUS, UMAT and VUMAT routines are provided to simulate the elastic-to-plastic behavior of Nitinol. This model is based on additive strain decomposition, in which the total strain experienced by the material is presented as the sum of the strain from the elastic region, the transformation region, and the plastic region. Superelastic-only behavior as well as superelastic-plastic behavior can both be implemented by incorporating different numbers of material parameters. Several key parameters include austenite elasticity, transformation strain, reference temperature, and martensite Poisson's ratio. ANSYS (ANSYS Inc, Cecil Township, PA) contains a material model for advanced SMAs based on generalized plasticity theory by Jia *et al.*[58] Similarly to ABAQUS, this model takes into account additive decomposition of total strain into the linearly elastic portion and a transformation component.

Despite the widespread incorporation of SMA constitutive models into FE codes, one of the main challenges is to determine the many material parameters that describe Nitinol behavior. Table 4 provides a summary of current literature that reports comprehensive sets of Nitinol material parameters that can be readily used in FEA.

SUMMARY

Unique shape memory and superelastic properties of Nitinol have allowed to significantly advance the development of minimally invasive endovascular treatment techniques using stents. However, despite the widespread successful use in other arterial beds, Nitinol stent

performance in the FPA continues to be associated with poor clinical outcomes as manifested by reduced patency rates and increased incidence of repeated surgical interventions that dramatically increase cost.[75] Although from a material standpoint there is a good understanding of basic physical and mechanical properties of Nitinol alloy, the understanding of how Nitinol stents behave as structures and how they interact with the arterial wall is insufficient and requires further research. Likewise, a better understanding of the dynamic environment of the FPA is crucial in order to improve the design and clinical performance of stents used to treat PAD.

Acknowledgments

FUNDING

This study was supported in part by the National Heart, Lung, And Blood Institute of the National Institutes of Health under Award Numbers R01 HL125736 and F32 HL124905.

References

1. Adam DJ, Beard JD, Cleveland T, Bell J, Bradbury AW, Forbes JF, Fowkes FGR, Gillepsie I, Ruckley CV, Raab G, Storkey H. Bypass versus angioplasty in severe ischaemia of the leg (BASIL): multicentre, randomised controlled trial. Lancet. 2005; 366:1925– 1934. [PubMed: 16325694]
2. Adlakha S, Sheikh M, Wu J, Burket MW, Pandya U, Colyer W, Eltahawy E, Cooper CJ. Stent fracture in the coronary and peripheral arteries. J Interv Cardiol. 2010; 23:411–419. [PubMed: 20806458]
3. Analysis AE. Stenting for peripheral artery disease of the lower extremities: an evidence-based analysis. Ont Health Technol Asses Ser. 2010; 10:1–88.
4. Ansari F, Pack LK, Brooks SS, Morrison TM. Design considerations for studies of the biomechanical environment of the femoropopliteal arteries. J Vasc Surg. 2013; 58:804–813. [PubMed: 23870198]
5. Association, American Diabetes, and A. D. Association. Peripheral arterial disease in people with diabetes. Diabetes Care. 2003; 26:3333–3341. [PubMed: 14633825]
6. ASTM. Standard test methods for in vitro pulsatile durability testing of vascular stents 1. Current. 2011. https://doi.org/10.1520/f2477-07.proper
7. Auricchio F, Taylor RL. Shape-memory alloys: modelling and numerical simulations of the finite-strain superelastic behavior. Comput Methods Appl Mech Eng. 1997; 143:175–194.
8. Auricchio F, Taylor RL, Lubliner J. Shape-memory alloys: macromodelling and numerical simulations of the superelastic behavior. Comput Methods Appl Mech Eng. 1997; 146:281–312.
9. Barras CDJ, Myers KA. Nitinol: its use in vascular surgery and other applications. EJVES Extra. 2010; 19:564–569.
10. Bartholomew J, Olin J. Pathophysiology of peripheral arterial disease and risk factors for its development. Cleve Clin J Med. 2006; 73:8–14. [PubMed: 16444911]
11. Bosiers MM. The Zilver® PTX® single arm study: 12- month results from the TASC C/D lesion subgroup. J Cardiovasc Surg (Torino). 2013; 54:115–122.
12. Boyd JG, Lagoudas DC. A thermodynamical constitutive model for shape memory materials. Part I. The monolithic shape memory alloy. Int J Plast. 1996; 12:805– 842.
13. Brinson LC, Lammering R. Finite element analysis of the behavior of shape memory alloys and their applications. Int J Solids Struct. 1993; 30:3261–3280.
14. Buehler W, Gilfrich J, Wiley R. Effects of low-temperature phase changes on the mechanical properties of alloys near composition TiNi. J Appl Phys. 1963; 34:1475– 1477.
15. Chang CH, Lin JW, Hsu J, Wu LC, Lai MS. Stent revascularization versus bypass surgery for peripheral artery disease in type 2 diabetic patients: an instrumental variable analysis. Sci Rep. 2016; 6:37177. [PubMed: 27857178]

16. Cheng CP, Choi G, Herfkens RJ, Taylor CA. The effect of aging on deformations of the superficial femoral artery resulting from hip and knee flexion: potential clinical implications. J Vasc Interv Radiol. 2010; 21:195–202. [PubMed: 20022767]
17. Cheng C, Wilson N, Hallett R. In vivo MR angiographic quantification of axial and twisting deformations of the superficial femoral artery resulting from maximum hip and knee flexion. J Vasc Interv Radiol. 2006; 17:979–987. [PubMed: 16778231]
18. Cimminiello C. PAD: epidemiology and pathophysiology. Thromb Res. 2002; 106:V295–V301. [PubMed: 12359342]
19. Cisse C, Zaki W, Ben Zineb T. A review of constitutive models and modeling techniques for shape memory alloys. Int J Plast. 2016; 76:244–284.
20. Comstock RJ, Buchheit TE, Somerday M, Wert JA. Modeling the transformation stress of constrained shape memory alloy single crystals. Acta Mater. 1996; 44:3505– 3514.
21. Conte MS, Bandyk DF, Clowes AW, Moneta GL, Seely L, Lorenz TJ, Namini H, Hamdan AD, Roddy SP, Belkin M, Berceli SA, DeMasi RJ, Samson RH, Berman SS. Results of PREVENT III: a multicenter, randomized trial of edifoligide for the prevention of vein graft failure in lower extremity bypass surgery. J Vasc Surg. 2006; 43:742–751. [PubMed: 16616230]
22. Conti, M., Marconi, M., Campanile, G., Reali, A., Adami, D., Berchiolli, R., Auricchio, F. Patient-specific finite element analysis of popliteal stenting. Meccanica. 2016. https://doi.org/10.1007/s11012-016-0452-9
23. Cragg A, Lund G, Rysavy J, Castaneda F, Castaneda-Zuniga W, Amplatz K. Nonsurgical placement of arterial endoprostheses: a new technique using nitinol wire. Radiology. 1983; 147:261–263. [PubMed: 6828742]
24. Dake MDMD. Nitinol stents with polymer-free paclitaxel coating for lesions in the superficial femoral and popliteal arteries above the knee: twelve-month safety and effectiveness results from the Zilver PTX single-arm clinical study. J Endovasc Ther. 2011; 18:613–623. [PubMed: 21992630]
25. Dake MD, Ansel GM, Jaff MR, Ohki T, Saxon RR, Smouse HB, Zeller T, Roubin GS, Burket MW, Khatib Y, Snyder SA, Ragheb AO, White JK, Machan LS. Paclitaxel-eluting stents show superiority to balloon angioplasty and bare metal stents in femoropopliteal disease: twelve-month zilver PTX randomized study results. Circ Cardiovasc Interv. 2011; 4:495–504. [PubMed: 21953370]
26. Darling JDJD. Results for primary bypass versus primary angioplasty/stent for lower extremity chronic limb-threatening ischemia. J Vasc Surg. 2017; 66:466–475. [PubMed: 28274753]
27. Deas DSJ, Marshall AP, Bian A, Shintani A, Guzman RJ. Association of cardiovascular and biochemical risk factors with tibial artery calcification. Vasc Med. 2015; 20:326–331. [PubMed: 25907899]
28. Desyatova A, MacTaggart J, Kamenskiy A. Constitutive modeling of human femoropopliteal artery biaxial stiffening due to aging and diabetes. Acta Biomater. 2017; 64:50–58. [PubMed: 28974476]
29. Desyatova, A., MacTaggart, J., Romarowski, R., Poulson, W., Conti, M., Kamenskiy, A. Effect of aging on mechanical stresses, deformations, and hemodynamics in human femoropopliteal artery due to limb flexion. Biomech Model Mechanobiol. 2017. https://doi.org/10.1007/s10237-017-0953-z
30. Desyatova A, Poulson W, Deegan P, Lomneth C, Seas A, Maleckis K, MacTaggart J, Kamenskiy A. Limb flexion-induced twist and associated intramural stresses in the human femoropopliteal artery. J R Soc Interface. 2017; 14:20170025. [PubMed: 28330991]
31. Dotter C, Buschmann R, Montgomery K, McKinney J. Transluminal expandable nitinol coil stent grafting: preliminary report. Radiology. 1983; 147:259–260. [PubMed: 6828741]
32. Drexel MJ, Selvaduray GS, Pelton AR. The effects of cold work and heat treatment on the properties of nitinol wire. Proc Int Conf Shape Mem Superelastic Technol. 2006
33. Duda SH, Wiskirchen J, Tepe G, Bitzer M, Kaulich TW, Stoeckel D, Claussen CD. Physical properties of endovascular stents: an experimental comparison. J Vasc Interv Radiol. 2000; 11:645–654. [PubMed: 10834499]
34. Duerig TW, Bhattacharya K. The influence of the R-phase on the superelastic behavior of NiTi. Shape Mem Superelasticity. 2015; 1:153–161.

35. Duerig T, Pelton A, Stöckel D. An overview of nitinol medical applications. Mater Sci Eng A. 1999; 273:149– 160.
36. Duerig TW, Tolomeo DE, Wholey M. An overview of superelastic stent design. Minim Invasive Ther Allied Technol. 2000; 9:235–246. [PubMed: 20156021]
37. Dyet JF, Watts WG, Ettles DF, Nicholson AA. Mechanical properties of metallic stents: how do these properties influence the choice of stent for specific lesions. Cardiovasc Interv Radiol. 2000; 23:47–54.
38. Elahinia MH, Hashemi M, Tabesh M, Bhaduri SB. Manufacturing and processing of NiTi implants: a review. Prog Mater Sci. 2012; 57:911–946.
39. Favier D, Liu Y, Orgéas L, Sandel A, Debove L, Comte-Gaz P. Influence of thermomechanical processing on the superelastic properties of a Ni-rich Nitinol shape memory alloy. Mater Sci Eng A. 2006; 429:130–136.
40. FDA. Non-clinical engineering tests and recommended labeling for intravascular stents and associated delivery systems. 2010
41. Frick CP, Ortega AM, Tyber J, Maksound AEM, Maier HJ, Liu Y, Gall K. Thermal processing of polycrystalline NiTi shape memory alloys. Mater Sci Eng A. 2005; 405:34–49.
42. Gabrielli R, Rosati MS, Chiappa R, Millarelli M, Marcuccio L, Siani A, Caselli G. First clinical experience with the innova versus the protege everflex self-expanding bare metal stents in superficial femoral artery occlusions. Thorac Cardiovasc Surg. 2015; 63:158–163. [PubMed: 25602844]
43. Ganguly A, Simons J, Schneider A, Keck B, Bennett NR, Herfkens RJ, Coogan SM, Fahrig R. In-vivo imaging of femoral artery nitinol stents for deformation analysis. J Vasc Interv Radiol. 2011; 22:244–249. [PubMed: 21276917]
44. Garcia L, Jaff MR, Metzger C, Sedillo G, Pershad A, Zidar F, Patlola R, Wilkins RG, Espinoza A, Iskander A, Khammar GS, Khatib Y, Beasley R, Makam S, Kovach R, Kamat S, Leon LRJ, Eaves WB, Popma JJ, Mauri L, Donohoe D, Base CC, Rosenfield K. Wire-interwoven nitinol stent outcome in the superficial femoral and proximal popliteal arteries: twelve-month results of the SUPERB trial. Circ Cardiovasc Interv. 2015; 8:1–8.
45. Glagov S, Weisenberg E, Zarins CK, Stankunavicius R, Kolettis GJ. Compensatory enlargement of human atherosclerotic coronary arteries. N Engl J Med. 1987; 316:1371–1375. [PubMed: 3574413]
46. Gökgöl C, Schumann S, Diehm N, Zheng G, Büchler P. In vivo quantification of the deformations of the femoropopliteal segment. J Endovasc Ther. 2017; 24:27–34. [PubMed: 28095767]
47. Gong, X., Pelton, A., Duerig, T. Finite element analysis and experimental evaluation of superelastic Nitinol stent. Proc. International Conference on Shape Memory and Superelastic Superelastic; 2004.
48. Goodney PP, Beck AW, Nagle J, Welch HG, Zwolak RM. National trends in lower extremity bypass surgery, endovascular interventions, and major amputations. J Vasc Surg. 2009; 50:54–60. [PubMed: 19481407]
49. Gray WA, Feiring A, Cioppi M, Hibbard R, Gray B, Khatib Y, Jessup D, Bachinsky W, Rivera E, Tauth J, Patarca R, Massaro J, Stoll H-P, Jaff MR. S.M.A.R.T. Self-expanding nitinol stent for the treatment of atherosclerotic lesions in the superficial femoral artery (STROLL): 1-year outcomes. J Vasc Interv Radiol. 2015; 26:21–28. [PubMed: 25454735]
50. Guzman RJ. Clinical, cellular, and molecular aspects of arterial calcification. J Vasc Surg. 2007; 45:57–63.
51. Ho CY, Shanahan CM. Medial arterial calcification: an overlooked player in peripheral arterial disease. Arterioscler Thromb Vasc Biol. 2016; 36:1475–1482. [PubMed: 27312224]
52. Humphrey JD. Vascular adaptation and mechanical homeostasis at tissue, cellular, and sub-cellular levels. Cell Biochem Biophys. 2008; 50:53–78. [PubMed: 18209957]
53. Humphrey JD, Eberth JF, Dye WW, Gleason RL. Fundamental role of axial stress in compensatory adaptations by arteries. J Biomech. 2009; 42:1–8. [PubMed: 19070860]
54. Irwin CL, Guzman RJ. Matrix metalloproteinases in medial arterial calcification: potential mechanisms and actions. Vascular. 2009; 17(Suppl 1):S40–S44. [PubMed: 19426608]

55. Kamenskiy AV I, Pipinos I, Dzenis YA, Lomneth CS, Kazmi SAJ, Phillips NY, MacTaggart JN. Passive biaxial mechanical properties and in vivo axial pre-stretch of the diseased human femoropopliteal and tibial arteries. Acta Biomater. 2014; 10:1301– 1313. [PubMed: 24370640]
56. Kamenskiy AV I, Pipinos I, Dzenis YA, Phillips NY, Desyatova AS, Kitson J, Bowen R, MacTaggart JN. Effects of age on the physiological and mechanical characteristics of human femoropopliteal arteries. Acta Biomater. 2015; 11:304–313. [PubMed: 25301303]
57. Kamenskiy, A., Poulson, W., Sim, S., Reilly, A., Luo, J., MacTaggart, J. Prevalence of calcification in human femoropopliteal arteries and its association with demographics, risk factors, and arterial stiffness. Atheroscler Thromb Vasc Biol. 2018. https://doi.org/10.1161/ATVBAHA.117.310490
58. Kamenskiy A, Seas A, Bowen G, Deegan P, Desyatova A, Bohlim N, Poulson W, Mactaggart J. In situ longitudinal pre-stretch in the human femoropopliteal artery. Acta Biomater. 2016; 32:231–237. [PubMed: 26766633]
59. Kamenskiy A, Seas A, Deegan P, Poulson W, Anttila E, Sim S, Desyatova A, MacTaggart J. Constitutive description of human femoropopliteal artery aging. Biomech Model Mechanobiol. 2017; 16:681–692. [PubMed: 27771811]
60. Kauffman GB, Mayo I. The story of nitinol: the serendipitous discovery of the memory metal and its applications. Chem Educ. 1997; 2(2):1–21.
61. Kleinstreuer C, Li Z, Basciano CA, Seelecke S, Farber MA. Computational mechanics of Nitinol stent grafts. J Biomech. 2008; 41:2370–2378. [PubMed: 18644312]
62. Kneissl AC, Unterweger E, Bruncko M, Lojen G, Mehrabi K, Scherngell H. Microstructure and properties of NiTi and CuAlNi shape memory alloys. Metalurgija. 2008; 14:89–100.
63. Krankenberg H, Schlüter M, Steinkamp HJ, Bürgelin K, Scheinert D, Schulte KL, Minar E, Peeters P, Bosiers M, Tepe G, Reimers B, Mahler F, Tübler T, Zeller T. Nitinol stent implantation versus percutaneous transluminal angioplasty in superficial femoral artery lesions up to 10 cm in length: the Femoral Artery Stenting Trial (FAST). Circulation. 2007; 116:285–292. [PubMed: 17592075]
64. Kurayev A, Zavlunova S, Babaev A. CRT-207 role of nitinol stent fractures in the development of in-stent restenosis in the superficial femoral artery. JACC Cardiovasc Interv. 2014; 7:S35.
65. Laird JR, Jain A, Zeller T, Feldman R, Scheinert D, Popma JJ, Armstrong EJ, Jaff MR. Nitinol stent implantation in the superficial femoral artery and proximal popliteal artery: twelve-month results from the complete SE multicenter trial. J Endovasc Ther. 2014; 21:202– 212. [PubMed: 24754279]
66. Laird JR, Katzen BT, Scheinert D, Lammer J, Carpenter J, Buchbinder M, Dave R, Ansel G, Lansky A, Cristea E, Collins TJ, Goldstein J, Cao AY, Jaff MR. Nitinol stent implantation vs. balloon angioplasty for lesions in the superficial femoral and proximal popliteal arteries of patients with claudication: three-year follow-up from the RESILIENT randomized trial. J Endovasc Ther. 2012; 19:1–9. [PubMed: 22313193]
67. Laird, JR., Yeo, KK. The treatment of femoropopliteal in-stent restenosis back to the future. J Am Coll Cardiol. 2012. https://doi.org/10.1016/j.jacc.2011.09.037
68. Lammer J, Zeller T, Hausegger KA, Schaefer PJ, Gschwendtner M, Mueller-Huelsbeck S, Rand T, Funovics M, Wolf F, Rastan A, Gschwandtner M, Puchner S, Ristl R, Schoder M. Heparin-bonded covered stents versus bare-metal stents for complex femoropopliteal artery lesions: the randomized VIASTAR trial (viabahn endoprosthesis with propaten bioactive surface [VIA] versus bare nitinol stent in the treatment of long lesions in sup. J Am Coll Cardiol. 2013; 62:1320–1327. [PubMed: 23831445]
69. Lehto S, Niskanen L, Suhonen M, Rönnemaa T, Laakso M. Medial artery calcification. A neglected harbinger of cardiovascular complications in non-insulin-dependent diabetes mellitus. Arterioscler Thromb Vasc Biol. 1996; 16:978–983. [PubMed: 8696962]
70. Levy PJ. Epidemiology and pathophysiology of peripheral arterial disease. Clin Cornerstone. 2002; 4:1–13.
71. Liistro F, Grotti S, Porto I, Angioli P, Ricci L, Ducci K, Falsini G, Ventoruzzo G, Turini F, Bellandi G, Bolognese L. Drug-eluting balloon in peripheral intervention for the superficial femoral artery: the DEBATE-SFA randomized trial (Drug Eluting Balloon in Peripheral Intervention for the Superficial Femoral Artery). JACC Cardiovasc Interv. 2013; 6:1295–1302. [PubMed: 24239203]

72. Liu X, Wang Y, Yang D, Qi M. The effect of ageing treatment on shape-setting and superelasticity of a nitinol stent. Mater Charact. 2008; 59:402–406.
73. MacTaggart JJN, Phillips NNY, Lomneth CCS, Pipinos III, Bowen R, Timothy Baxter B, Johanning J, Matthew Longo G, Desyatova AAS, Moulton MMJ, Dzenis YAY, Kamenskiy AAV, Baxter B, Johanning J, Longo G, Desyatova AAS, Moulton MMJ, Dzenis YAY, Kamenskiy AAV. Three-dimensional bending, torsion and axial compression of the femoropopliteal artery during limb flexion. J Biomech. 2014; 47:2249–2256. [PubMed: 24856888]
74. MacTaggart J, Poulson W, Seas A, Deegan P, Lomneth C, Desyatova A, Maleckis K, Kamenskiy A. Stent design affects femoropopliteal artery deformation. 2018
75. Mahoney EM, Wang K, Keo HH, Duval S, Smolderen KG, Cohen DJ, Steg G, Bhatt DL, Hirsch AT. Vascular hospitalization rates and costs in patients with peripheral artery disease in the United States. Circ Cardiovasc Qual Outcomes. 2010; 3:642–651. [PubMed: 20940249]
76. Mahtabi MJ, Shamsaei N. Multiaxial fatigue modeling for Nitinol shape memory alloys under in-phase loading. J Mech Behav Biomed Mater. 2016; 55:236–249.
77. Mahtabi MJ, Shamsaei N, Mitchell MR. Fatigue of Nitinol: the state-of-the-art and ongoing challenges. J Mech Behav Biomed Mater. 2015; 50:228–254. [PubMed: 26160028]
78. Maleckis K, Deegan P, Poulson W, Sievers C, Desyatova A, MacTaggart J, Kamenskiy A. Comparison of femoropopliteal artery stents under axial and radial compression, axial tension, bending, and torsion deformations. J Mech Behav Biomed Mater. 2017; 75:160– 168. [PubMed: 28734257]
79. Matsumura JS, Yamanouchi D, Goldstein JA, Pollock CW, Bosiers M, Schultz GA, Scheinert D, Rocha-Singh KJ. The United States StuDy for EvalUating EndovasculaR TreAtments of Lesions in the Superficial Femoral Artery and Proximal Popliteal By usIng the Protégé EverfLex NitInol STent SYstem II (DURABILITY II). J Vasc Surg. 2013; 58:73–83.e1. [PubMed: 23642924]
80. Mohr PJPJ. Clinical outcomes of endovascular treatment of TASC-II C and D femoropopliteal lesions with the Viabahn endoprosthesis. Cardiovasc Revascularization Med. 2015; 16:465–468.
81. Montero-Baker MM. Analysis of endovascular therapy for femoropopliteal disease with the Supera stent. J Vasc Surg. 2016; 64:1002–1008. [PubMed: 27444365]
82. Müller-Hülsbeck S, Schäfer PJ, Charalambous N, Yagi H, Heller M, Jahnke T. Comparison of second-generation stents for application in the superficial femoral artery: an in vitro evaluation focusing on stent design. J Endovasc Ther. 2010; 17:767–776. [PubMed: 21142489]
83. Mwipatayi BP, Hockings A, Hofmann M, Garbowski M, Sieunarine K. Balloon angioplasty compared with stenting for treatment of femoropopliteal occlusive disease: a meta-analysis. J Vasc Surg. 2008; 47:461–469. [PubMed: 17950563]
84. Nagl F, Siekmeyer G, Quellmalz M, Schuessler A. A comparison of different nitinol material data sources for finite element analysis. J Mater Eng Perform. 2011; 20:737–744.
85. Nakazawa G, Finn AV, Vorpahl M, Ladich E, Kutys R, Balazs I, Kolodgie FD, Virmani R. Incidence and predictors of drug-eluting stent fracture in human coronary artery. A pathologic analysis. J Am Coll Cardiol. 2009; 54:1924–1931. [PubMed: 19909872]
86. Nasser F, Kambara A, Abath C, Cavalcanti D, Barros I, Pires N, Rivera M, Neser A, Ingrund J, Burihan M, Silveira P, Galego G, Bortoluzzi C, Franklin R, Bosiers M, Deloose K, Razuk A, Caffaro R, Karakhanian WK, Park J, Lopes C, Pinto D, Bez L, Lopes R, Mourao A, Kleinsorge G. Safety and efficacy of the EPIC nitinol vascular stent system for the treatment of lesions located in the superficial femoral artery: prospective and multicentric trial. J Cardiovasc Surg (Torino). 2015; 58:409–415.
87. Nematzadeh F, Sadrnezhaad SK. Effects of material properties on mechanical performance of Nitinol stent designed for femoral artery: finite element analysis. Sci Iran. 2012; 19:1564–1571.
88. Ng KL, Sun QP. Stress-induced phase transformation and detwinning in NiTi polycrystalline shape memory alloy tubes. Mech Mater. 2006; 38:41–56.
89. Ni Ghriallais R, Heraty K, Smouse B, Burke M, Gilson P, Bruzzi M. Deformation of the femoropopliteal segment: effect of stent length, location, flexibility, and curvature. J Endovasc Ther. 2016; 23:907–918. [PubMed: 27647689]

90. Nikanorov A, Schillinger M, Zhao H, Minar E, Schwartz LB. Assessment of self-expanding nitinol stent deformation after chronic implantation into the femoropopliteal arteries. EuroIntervention. 2013; 9:730–737. [PubMed: 24169133]
91. Nikanorov A, Smouse HB, Osman K, Bialas M, Shrivastava S, Schwartz LB. Fracture of self-expanding nitinol stents stressed in vitro under simulated intravascular conditions. J Vasc Surg. 2008; 48:435–440. [PubMed: 18486426]
92. Nishida M, Wayman CM, Honma T. Precipitation processes in near-equiatomic TiNi shape memory alloys. Metall Trans A. 1986; 17:1505–1515.
93. Ohki T, Angle JF, Yokoi H, Jaff MR, Popma J, Piegari G, Kanaoka Y. One-year outcomes of the U.S. and Japanese regulatory trial of the Misago stent for treatment of superficial femoral artery disease (OSPREY study). J Vasc Surg. 2016; 63:370–376. [PubMed: 26483003]
94. Otsuka K, Ren X. Physical metallurgy of Ti–Ni-based shape memory alloys. Prog Mater Sci. 2005; 50:511–678.
95. Patoor, E., Eberhardt, A., Berveiller, M. Micromechanical modelling of superelasticity in shape memory alloys. Shape Mem Alloy J Phys IV Colloq. 1996. https://doi.org/10.1051/jp4:1996127
96. Pelton AR. Fatigue and durability of nitinol stents. J Mech Behav Biomed Mater. 2007; 1:153–164. [PubMed: 19627780]
97. Pelton A, Rebelo N, Duerig T, Wick A. Experimental and FEM analysis of the bending behaviour of superelastic tubing experimental and FEM analysis of the bending behavior of super elastic tubing. Proc First Int Conf Shape Mem Superelastic Technol. 1994:353–358.
98. Petrini L, Trotta A, Dordoni E, Migliavacca F, Dubini G, Lawford PV, Gosai JN, Ryan DM, Testi D, Pennati G. A computational approach for the prediction of fatigue behaviour in peripheral stents: application to a clinical case. Ann Biomed Eng. 2016; 44:536–547. [PubMed: 26433586]
99. Poulson, W., Kamenskiy, A., Seas, A., Deegan, P., Lomneth, C., MacTaggart, J. Limb flexion-induced axial compression and bending in human femoropopliteal artery segments. J Vasc Surg. 2017. https://doi.org/10.1016/j.jvs.2017.01.071
100. Powell RJRJ. Stent placement in the superficial femoral and proximal popliteal arteries with the innova self-expanding bare metal stent system. Catheter Cardiovasc Interv. 2017; 89:1069–1077. [PubMed: 28296239]
101. Price PA, Faus SA, Williamson MK. Warfarin-induced artery calcification is accelerated by growth and vitamin D. Arterioscler Thromb Vasc Biol. 2000; 20:317–327. [PubMed: 10669626]
102. Qi, Y., Qi, H., He, Y., Lin, W., Li, P., Qin, L., Hu, Y., Chen, L., Liu, Q., Sun, H., Liu, Q., Zhang, G., Cui, S., Hu, J., Yu, L., Zhang, D., Ding, J. Strategy of metal–polymer composite stent to accelerate biodegradation of iron-based biomaterials. ACS Appl Mater Interfaces. 2017. https://doi.org/10.1021/acsami.7b15206
103. Qin X, Corriere MA, Matrisian LM, Guzman RJ. Matrix metalloproteinase inhibition attenuates aortic calcification. Arterioscler Thromb Vasc Biol. 2006; 26:1510–1516. [PubMed: 16690876]
104. Rebelo N, Walker N, Foadian H. Simulation of implantable nitinol stents. 2001
105. Robertson SW, Gong XY, Ritchie RO. Effect of product form and heat treatment on the crystallographic texture of austenitic Nitinol. J Mater Sci. 2006; 41:621–630.
106. Robertson SW, Pelton AR, Ritchie RO. Mechanical fatigue and fracture of Nitinol. Int Mater Rev. 2012; 57:1–37.
107. Robertson, SW., Ritchie, RO., Mehta, A., Gong, XY., Pelton, AR. Ultrahigh-resolution in situ diffraction characterization of the local mechanics at a growing crack tip in Nitinol. SMST-2006 Proc. Int. Conf. Shape Mem. Superelastic Technol; 2008.
108. Rocha-Singh KJ, Zeller T, Jaff MR. Peripheral arterial calcification: prevalence, mechanism, detection, and clinical implications. Catheter Cardiovasc Interv. 2014; 83:212–220.
109. Rundback JH, Herman KC, Patel A. Superficial femoral artery intervention: creating an algorithmic approach for the use of old and novel (endovascular) technologies. Curr Treat Options Cardiovasc Med. 2015; 17:400. [PubMed: 26265117]
110. Ryhänen J, Ryhanen J. Minimally invasive therapy & allied technologies biocompatibility of nitinol biocompatibility of Nitinol. Minim Invasive Ther Allied Technol. 2000; 9:99–105.

111. Scheinert D, Scheinert S, Sax J, Piorkowski C, Bräunlich S, Ulrich M, Biamino G, Schmidt A. Prevalence and clinical impact of stent fractures after femoropopliteal stenting. J Am Coll Cardiol. 2005; 45:312–315. [PubMed: 15653033]
112. Schillinger M, Minar E. Past, present and future of femoropopliteal stenting. J Endovasc Ther. 2009; 16:147–152. [PubMed: 19456195]
113. Schillinger M, Sabeti S, Dick P, Amighi J, Mlekusch W, Schlager O, Loewe C, Cejna M, Lammer J, Minar E. Sustained benefit at 2 years of primary femoropopliteal stenting compared with balloon angioplasty with optional stenting. Circulation. 2007; 115:2745–2749. [PubMed: 17502568]
114. Schillinger M, Sabeti S, Loewe C. Balloon angioplasty versus implantation of nitinol stents in the superficial femoral artery. N Engl J Med. 2006; 354:1879–1888. [PubMed: 16672699]
115. Schlager O, Dick P, Sabeti S, Amighi J, Mlekusch W, Minar E, Schillinger M. Long-segment SFA stenting-the dark sides: in-stent restenosis, clinical deterioration, and stent fractures. J Endovasc Ther. 2005; 12:676–684. [PubMed: 16363897]
116. Sharma U, Concagh D, Core L, Kuang Y, You C, Pham Q, Zugates G, Busold R, Webber S, Merlo J, Langer R, Whitesides GM, Palasis M. The development of bioresorbable composite polymeric implants with high mechanical strength. Nat Mater. 2017; 17:96. [PubMed: 29180778]
117. Sibé M, Kaladji A, Boirat C, Cardon A, Chaufour X, Bossavy JP, Saint-Lebes B. French multicenter experience with the GORE TIGRIS vascular stent in superficial femoral and popliteal arteries. J Vasc Surg. 2017; 65:1329–1335. [PubMed: 28222987]
118. Sitepu H. Use of synchrotron diffraction data for describing crystal structure and crystallographic phase analysis of R-phase NiTi shape memory alloy. Textures Microstruct. 2003; 35:185–195.
119. Smouse BHB, Nikanorov A, Laflash D. Biomechanical forces in the femoropopliteal arterial segment. Endovasc Today. 2005; 4:60–66.
120. Stankiewicz JM, Robertson SW, Ritchie RO. Fatigue-crack growth properties of thin-walled superelastic austenitic Nitinol tube for endovascular stents. J Biomed Mater Res A. 2007; 81:685–691. [PubMed: 17187394]
121. Stoeckel D, Pelton A, Duerig T. Self-expanding nitinol stents: material and design considerations. Eur Radiol. 2004; 14:292–301. [PubMed: 12955452]
122. Stone PAPA. Early results with LifeStent implantation in RESILIENT and non-RESILIENT inclusion criteria patients. Vascular. 2015; 23:225–233. [PubMed: 25121510]
123. Sullivan SJL, Dreher ML, Zheng J, Chen L, Madamba D, Miyashiro K, Trépanier C, Nagaraja S. Effects of oxide layer composition and radial compression on nickel release in Nitinol stents. Shape Mem Superelasticity. 2015; 1:319–327.
124. Sun QP, Hwang KC. Micromechanics modelling for the constitutive behavior of polycrystalline shape memory alloys—I. Derivation of general relations. J Mech Phys Solids. 1993; 41:1–17.
125. Thériault P, Terriault P, Brailovski V, Gallo R. Finite element modeling of a progressively expanding shape memory stent. J Biomech. 2006; 39:2837–2844. [PubMed: 16259989]
126. Timmins LH, Miller MW, Clubb FJ, Moore JE. Increased artery wall stress post-stenting leads to greater intimal thickening. Lab Investig. 2011; 91:955–967. [PubMed: 21445059]
127. Virmani R, Farb A. Pathology of in-stent restenosis. Curr Opin Lipidol. 1999; 10:499–506. [PubMed: 10680043]
128. Gore WL. Associates. I. Mechanical properties of nitinol stents and stent-grafts: comparison of 6 mm diameter devices. 2007
129. Watt J. Origin of femoro-popliteal occlusions. Br Med J. 1965; 2:1455–1459. [PubMed: 5849435]
130. Werner MM. SUMMIT registry: one-year outcomes after implantation of the EPIC self-expanding nitinol stent in the femoropopliteal segment. J Endovasc Ther. 2013; 20:759– 766. [PubMed: 24325691]
131. Werner M. Factors affecting reduction in SFA stent fracture rates. Endovasc Today. 2014; 13:93–95.
132. Werner M, Micari A, Cioppa A, Vadalà G, Schmidt A, Sievert H, Rubino P, Angelini A, Scheinert D, Biamino G. Evaluation of the biodegradable peripheral Igaki-Tamai stent in the treatment of de novo lesions in the superficial femoral artery: the GAIA study. JACC Cardiovasc Interv. 2014; 7:305–312. [PubMed: 24529932]

133. Whitcher FD. Simulation of in vivo loading conditions of nitinol vascular stent structures. Comput Struct. 1997; 64:1005–1011.

134. Yeung KWK, Cheung KMC, Lu WW, Chung CY. Optimization of thermal treatment parameters to alter austenitic phase transition temperature of NiTi alloy for medical implant. Mater Sci Eng A. 2004; 383:213–218.

135. Zeller T, Saratzis N, Scheinert D, Minar E, Beregi JP, Schillinger M, Hausegger HA, Amor M, Quaretti P, Moratto R, Dorange C, Boone E, Krankenberg H. Non-randomized, prospective, multi-centre evaluation of the ABSOLUTE .035 peripheral self-expanding stent system for occluded or stenotic superficial femoral or proximal popliteal arteries (ASSESS Trial): acute and 30-day results. J Cardiovasc Surg (Torino). 2007; 48:719–726.

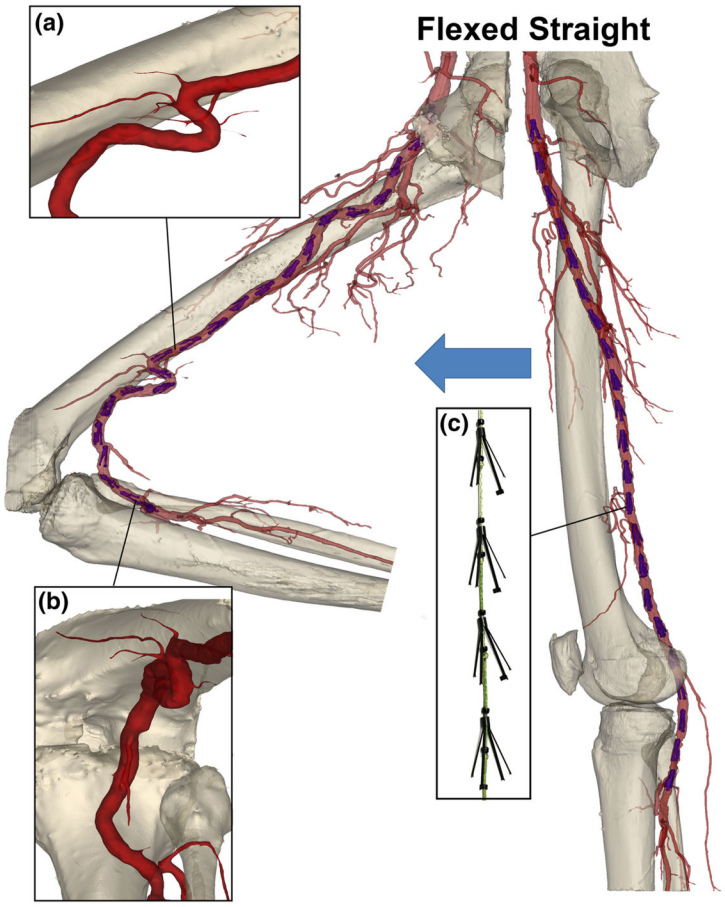

FIGURE 1.

Deformations of the FPA with limb flexion in a human cadaver model. Inserts demonstrate severe deformations of the artery at the adductor hiatus (a) and in the popliteal segment below the knee (b). Intra-arterial markers used to quantify FPA deformations with limb flexion are presented in the insert (c).

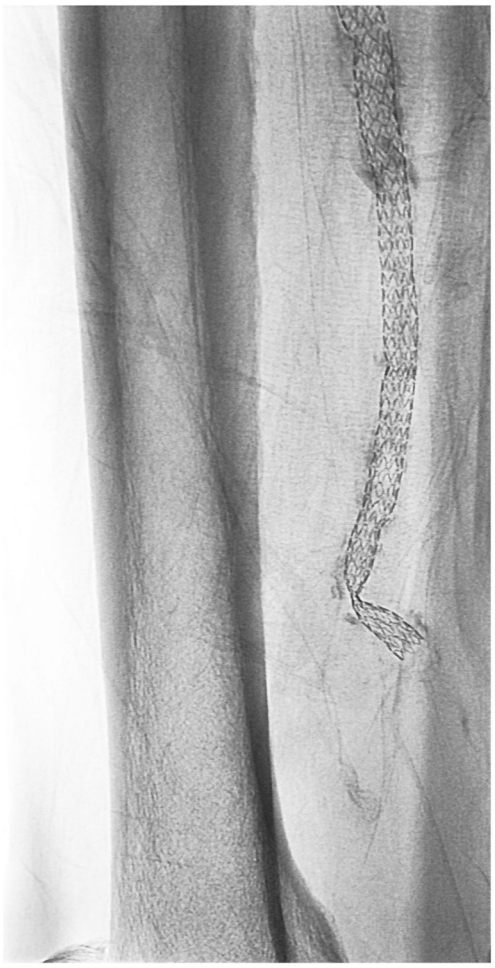

FIGURE 2.
Irreversible deformation of the balloon-expandable iCAST stent in the FPA.

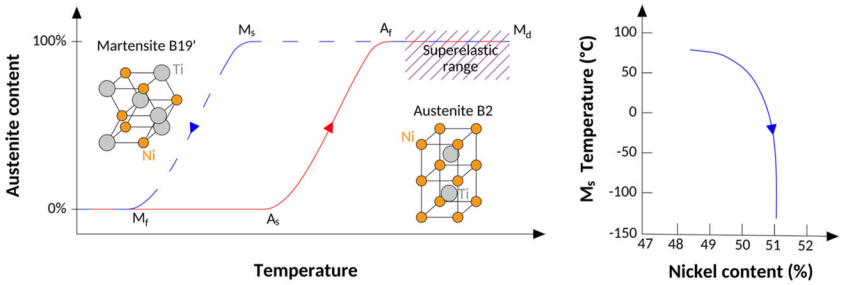

FIGURE 3.

Thermal phase transitions of Nitinol. Left: Temperature hysteresis of austenite and martensite transitions, Right: effect of elemental composition on M_s transition temperature.

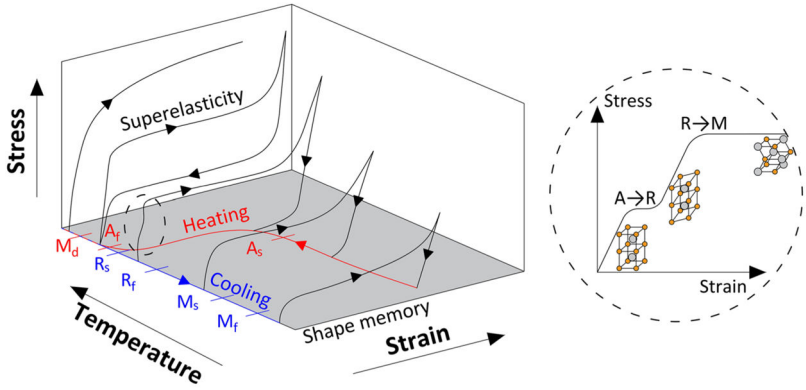

FIGURE 4.

Effect of temperature on mechanical properties of Nitinol. Insert on the right schematically represents the R-phase illustrating unit cell elongation along the [111] direction. More detailed crystallographic description of the R-phase can be found elsewhere.[94,118]

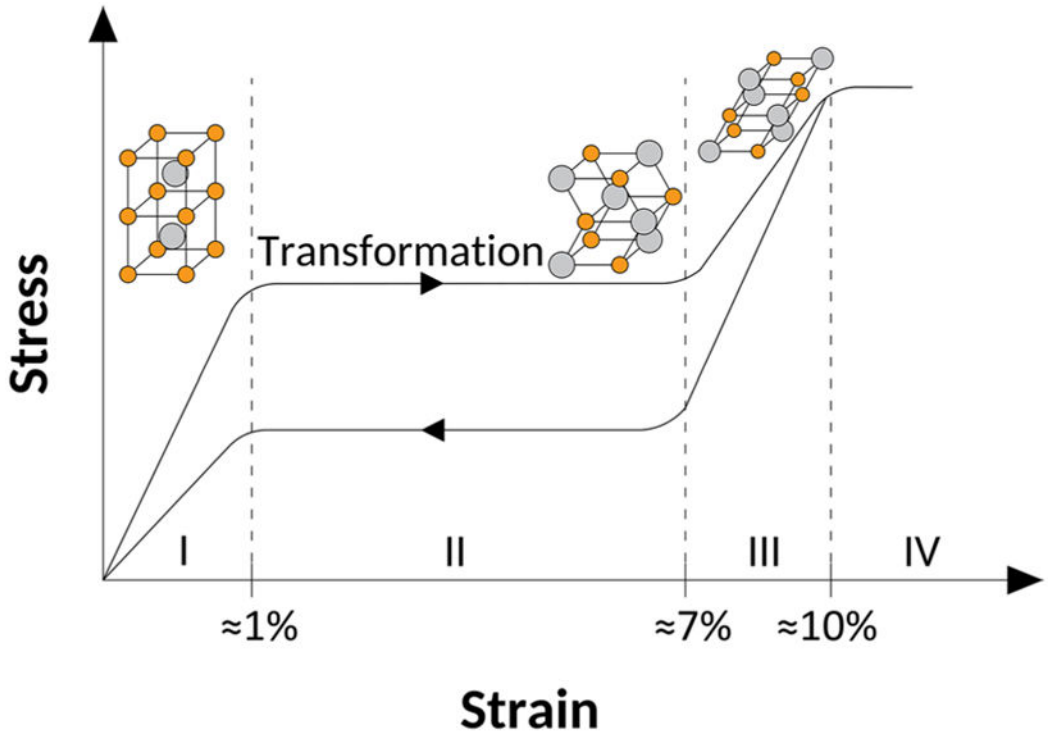

FIGURE 5.
Deformation behavior of Nitinol alloy in its superelastic form with corresponding microstructure.

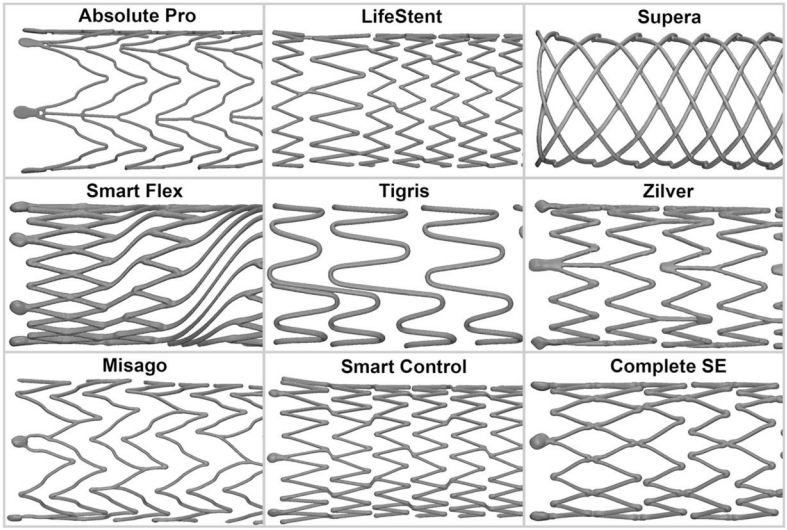

FIGURE 6.
Design patterns for some commonly used PAD stents.

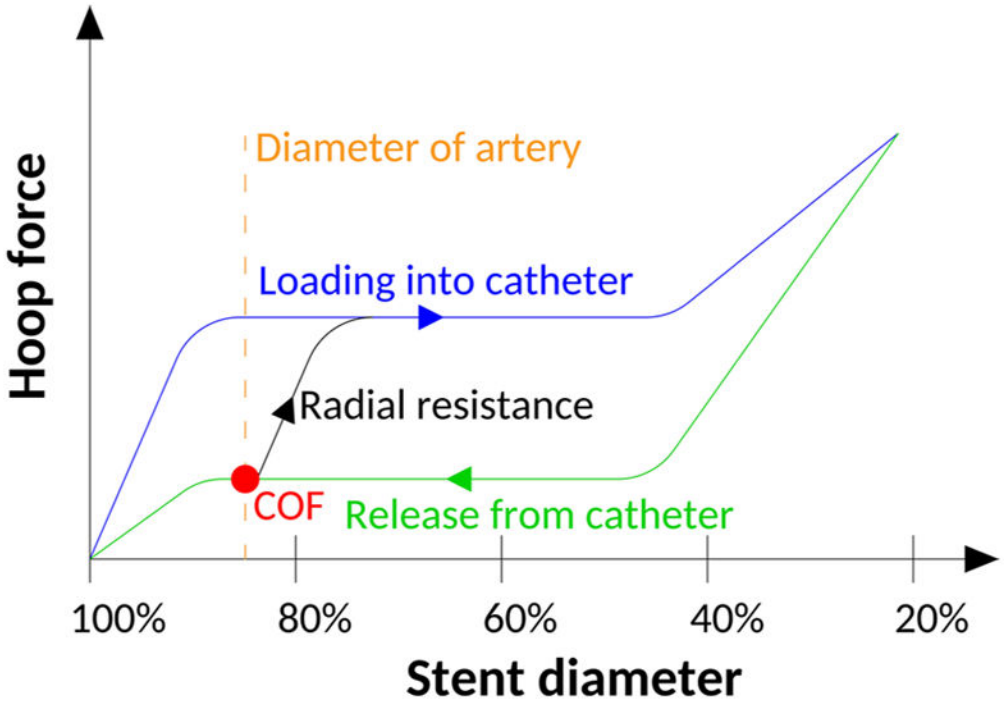

FIGURE 7.
Biomechanical performance of self-expanding Nitinol stents.

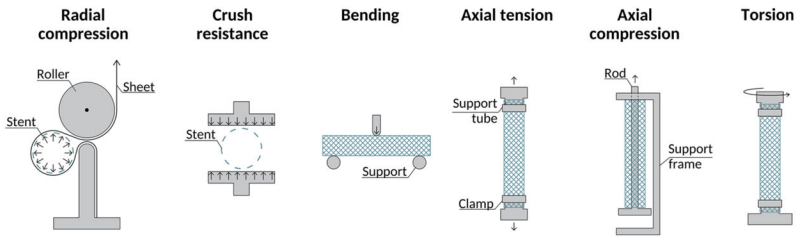

FIGURE 8.
Schematics of typical test setups used in mechanical characterization of stents.

TABLE 1

Results of clinical trials demonstrating 12-month patency rates for different FPA stents.

Device & company (trial)	12-month primary patency, %	Year
Luminexx Bard (FAST)[63]	68.3	2007
Absolute Abbott (ASSESS)[135]	90.7 (1-month patency)	2007
Zilver PTX Cook Medical[11,24,25]	77.6–86.2[a]	2011, 2011, 2013
LifeStent Bard (RESILIENT)[66,122]	81–81.5	2012, 2015
Maris Medtronic (DEBATE SFA)[71]	57.7	2013
Protégé Everflex Covidien (Durability II)[79]	67.7	2013
EPIC Boston Scientific (EPIC)[86,130]	76.1–85.1	2013, 2015
Heparin-Bonded Viabahn Gore (VIASTAR)[68,80]	74.8–78	2013, 2015
Complete SE Medtronic (Complete SE study)[65]	72.6	2014
Innova Boston Scientific[42,100]	43.3–66.4	2015, 2017
Cordis S.M.A.R.T (STROLL)[49]	71.2	2015
Supera Abbott (SUPERB)[44,81]	72.7–89.8	2015, 2016
Misago Terumo (OSPREY)[93]	82.9	2016
GORE Tigris[117]	81.5	2016

[a]Drug-eluting Stent coated with Paclitaxel.

TABLE 2

Average number of cycles until fracture under bending, axial compression, and torsion deformations for different stents tested in air.[82]

Stent model	Bending	Compression	Torsion
Misago	536,000 (1/5)	650,000 (0/5)	650,000 (0/5)
Absolute	456,667 (2/3)	23,333 (3/3)	60,000 (1/1)
Smart	41,667 (3/3)	3182 (3/3)	10,000 (1/1)
Luminexx	2415 (3/3)	1000 (3/3)	1000 (1/1)
Sentinol	16,400 (3/3)	6515 (3/3)	60,000 (1/1)
LifeStent	650,000 (0/1)	48,995 (1/1)	60,000 (1/1)
Sinus-SuperFlex	5000 (1/1)	4445 (1/1)	5000 (1/1)

Numbers in brackets indicate how many of the tested stents fractured before reaching 650,000 cycles.

TABLE 3

Stents fracture rates under 5% axial compression and 48° bending deformations repeated 10^7 cycles in silicone tubes.[91]

Stent model	Fracture under axial compression	Fracture under bending
Luminexx	4/5	5/5
Protégé Everflex	0/5	5/5
Smart Control	0/5	5/5
Xceed	2/9	4/9
LifeStent FlexStar	2/7	0/4
Absolute	1/30	1/30

TABLE 4

Summary of articles describing Nitinol mechanical properties that can be readiliy used in FEA of stents.

Authors/year	Description
Boyd and Lagoudas[12] (1996)	Developed a thermodynamic constitutive model for SMAs; provided material parameters for Nitinol
Auricchio and Taylor[7] (1997)	Developed a constitutive model that captured superelasticity of SMAs at finite strains; It was further developed by Aurrichio (2001) to include a time discrete solution algorithm; Contains material parameters for Nitinol from two uniaxial tension tests
Auricchio *et al.*[8] (1997)	Improved original model by using generalized plasticity for better description of one- and three-dimensional SMA behavior; this model is implemented in ABAQUS UMAT/VUMAT
Dyet *et al.*[37] (2000)	Assessed radial force, flexibility, radio-opacity, and trackability of Nitinol stents
Rebelo *et al.*[104] (2001)	Reported Nitinol properties used in ABAQUS UMAT/VUMAT subroutines. Properties were derived from an unknown type of Nitinol stent
Gong *et al.*[47] (2004)	Compared experimental and FE assessments of a Nitinol stent
Favier *et al.*[39] (2006)	Reported properties of Nitinol tubing with respect to thermomechanical processing; Evolution of properties was obtained from Differential Scanning Calorimetry measurements and tensile testing at elevated temperatures
Thériault and Terriault *et al.*[125] (2006)	Used a multilinear isotropic hardening law with Von Mises plasticity criteria to describe Nitinol behavior
Kleinstreuer *et al.*[61] (2008)	FE was performed on stent-grafts used for abdominal aortic aneurysms. Nitinol properties were obtained for tube samples heat-treated the same way as Medtronic stents
Nagl *et al.*[84] (2011)	Compared FE simulations using Nitinol properties that were obtained from different published sources
Nematzadeh and Sadrnezhaad[87] (2012)	Performed FE on a segment of an idealized stent subjected to crush resistance testing to evaluate effects of Nitinol properties